Scudder et al. Progress in Earth and Planetary Science (2016) 3:1
DOI 10.1186/s40645-015-0077-y

Progress in Earth and Planetary Science
a SpringerOpen Journal

REVIEW Open Access

Geochemical approaches to the quantification of dispersed volcanic ash in marine sediment

Rachel P. Scudder[1,6*], Richard W. Murray[1], Julie C. Schindlbeck[2], Steffen Kutterolf[2], Folkmar Hauff[2], Michael B. Underwood[3], Samantha Gwizd[4], Rebecca Lauzon[5] and Claire C. McKinley[6]

Abstract

Volcanic ash has long been recognized in marine sediment, and given the prevalence of oceanic and continental arc volcanism around the globe in regard to widespread transport of ash, its presence is nearly ubiquitous. However, the presence/absence of very fine-grained ash material, and identification of its composition in particular, is challenging given its broad classification as an "aluminosilicate" component in sediment. Given this challenge, many studies of ash have focused on discrete layers (that is, layers of ash that are of millimeter-to-centimeter or greater thickness, and their respective glass shards) found in sequences at a variety of locations and timescales and how to link their presence with a number of Earth processes. The ash that has been mixed into the bulk sediment, known as dispersed ash, has been relatively unstudied, yet represents a large fraction of the total ash in a given sequence. The application of a combined geochemical and statistical technique has allowed identification of this dispersed ash as part of the original ash contribution to the sediment. In this paper, we summarize the development of these geochemical/statistical techniques and provide case studies from the quantification of dispersed ash in the Caribbean Sea, equatorial Pacific Ocean, and northwest Pacific Ocean. These geochemical studies (and their sedimentological precursors of smear slides) collectively demonstrate that local and regional arc-related ash can be an important component of sedimentary sequences throughout large regions of the ocean.

Keywords: Dispersed ash, Caribbean Sea, Equatorial Pacific Ocean, Northwest Pacific Ocean, Ash layers, Volcanic eruptions, DSDP, ODP, IODP

Introduction

In the modern era, marine scientists' interest in volcanic ash can be traced back at least to the *HMS Challenger* expedition (1872–1876). Indeed, "What is marine sediment made of?" is a question that has been asked for 100s of years, and while many aspects of the petrology, mineralogy, and geochemistry of marine sediment have been well characterized, it is remarkable how much remains unknown about some key aspects of ocean mud. In particular, the presence/absence and composition of volcanic ash is challenging given its fine grain size, broad classification as an "aluminosilicate", and common presence, especially since both oceanic and continental arc volcanism are often located physically adjacent to oceanic environments and are known to globally generate and transport widespread ash (Fig. 1). Certainly, civilization's natural curiosity about volcanism has driven interest in the marine records of ash for generations of scientists. Additionally, these studies considered how to link their presence with explosive volcanism, climate, arc evolution, biological productivity, and other geological processes, as described below. Although the term "ash" is normally used in volcanology as a grain size definition (32 μm to 2 mm, e.g., Fisher and Schmincke 1984) for explosive volcanic products (juvenile matter and lithic fragments), we here use the term "ash" to indicate a product (mostly volcanic glass) from explosive volcanism

* Correspondence: rscudder@tamu.edu
[1]Department of Earth & Environment, Boston University, Boston, MA 02215, USA
[6]Department of Oceanography, Texas A&M University, College Station, TX 77843, USA
Full list of author information is available at the end of the article

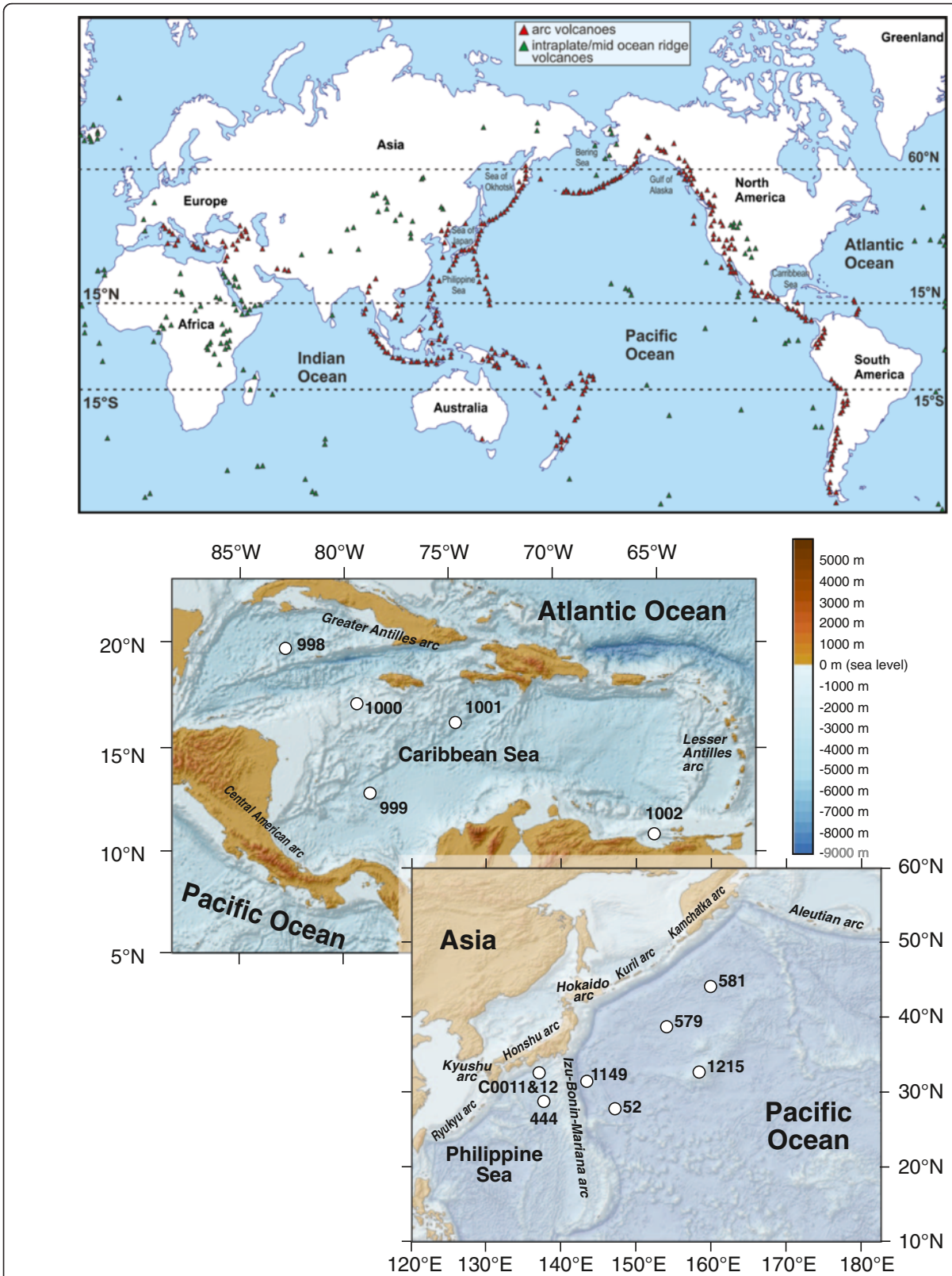

Fig. 1 (*Top*) Global distribution of subaerial volcanoes in different tectonic settings. Map has been modified after http://d-maps.com and volcano positions are taken from the Smithsonian Global Volcanism Program (http://www.volcano.si.edu). (*Bottom*) Locations of sites highlighted in this paper. Data from GeoMapApp (http://www.geomapapp.org); *GMRT* Global Multi-Resolution Topography (Ryan et al. 2009)

no matter which grain size a particle may have. Therefore, in this paper we refer to "discrete ash layers" as a volcanic product that is present as a clearly visible bed in the marine sediments (that is, ash layers of millimeter-to-centimeter or greater thickness, Fig. 2a–f) and their respective glass shards (Fig. 2g–l)) found in sequences at a variety of locations and timescales.

Less widely recognized than the discrete layers of ash is what has been referred to as "dispersed" ash. "Dispersed ash" is defined as volcanic ash material of various grain sizes (including single μm grains) that is mixed throughout the bulk sediment. This ash occurs in addition to the discrete ash layers. The presence of dispersed ash in the marine record has previously been relatively overlooked as it is difficult to identify petrographically due to its commonly extremely fine grain size (Rose et al. 2003, and references therein) and/or alteration to authigenic clay (Sigurdsson et al. 1997; Plank et al. 2000). Such alteration (e.g., Schacht et al. 2008) often results in fine-grained material that is unable to be differentiated from detrital terrigenous clay (non-ash, derived from land) on the basis of visual study alone.

Dispersed ash is the result from bioturbation of pre-existing discrete ash layers, the settling of airborne or subaqueous ash through the water column, transport by rivers and currents from terrestrially exposed ash deposits, and other processes (e.g., gravity flows). Because dispersed ash has often been only qualitatively addressed (e.g., via sedimentological smear slides), however it still plays as vital a role as discrete ash layers in many studies on multiple spatial and temporal scales, including (but not limited to) the following:

- Ash plays an important role for geochemical budgets (e.g., "Subduction Factory"), in that studies of geochemical recycling will benefit from an increased understanding of both input (subduction) and output (volcanism) fluxes (e.g., Straub 1997, 2008; Plank and Langmuir 1998; Straub and Schmincke 1998; Bryant et al. 1999, 2003; Straub and Layne 2002, 2003a,b; Hauff et al. 2003; Straub et al. 2004; Stern et al. 2006; Plank et al. 2007; Scudder et al. 2009, 2014; Tamura et al. 2009; Völker et al. 2011, 2014; Freundt et al. 2014). The amount, distribution, and composition of ash in sediment speaks to inputs as well as outputs in the budget, namely, knowing how much ash is entering the Subduction Factory is important for understanding recycling of geological material. Additionally, the ash record in the sediment itself provides an archive of local, regional, and global magmatic evolution.
- The marine repository of explosive volcanic eruptions is a vital record from which the geological history of arc evolution is recorded (e.g., Kennett et al. 1977; Ninkovich et al 1978; Sigurdsson et al. 1980, 2000; Huang 1980; Cambray et al. 1993, 1995; Lee et al. 1995; Bailey 1996; Peters et al. 2000; Straub 2003; Kutterolf et al. 2008a,b,c; Straub et al. 2009, 2010, 2015). An improved understanding of arc evolution has the potential to contribute significantly to knowledge regarding the birth, life, and death of arc magmatism. Furthermore, a full accounting of the ash record (that is, comparison of the dispersed ash record with that of the discrete layers) may provide information about arc evolution and erosional histories of landmasses. Studies of ash distribution are also vitally important to document risk associated with volcanic hazards.
- Reconstructions of eruption intensities and atmospheric wind patterns have been based on grain size characteristics and inferred dispersal patterns of the ash found in discrete layers, both at sea and on land (e.g., Huang et al. 1973, 1975; Shaw et al. 1974; Ledbetter and Sparks 1979; Carey and Sigurdsson 1980, 2000; Carey and Sparks 1986; Reid et al. 1996; Rose et al. 2003; Carey et al. 2010). These finer particles are probably the main constituent of dispersed ash, and therefore documenting the distribution of dispersed ash will constrain inferences of the transport pathways of volcanic material.
- The ability to quantify the amount of dispersed ash will increase knowledge of sedimentary physical properties (e.g., Peacock 1990; Kastner et al. 1991; Underwood and Pickering 1996; Chan and Kastner 2000; Saffer et al. 2008, 2012; Hüpers et al. 2015). Given that ash alters to clay in a hydration reaction, the amount of water bound in the sediment will increase, thus decreasing the shear strength of the mud. Additionally, the fluid budget of subducting sediment will be affected by these and, further, hydration/dehydration reactions. A quantification of the amount of dispersed ash will thus assist interpretation of physical properties of marine sediment and subduction zone modeling.
- Volcanic ash and eolian dust input to the surface ocean contributes nutrients to the surface ocean and are thus important for understanding trace metal cycling, biological productivity, climate change, volcano-climate interactions, and allied biogeochemical studies (e.g., Huang et al. 1974; Shaw et al. 1974; Carey 1997; Frogner et al. 2001; Jones and Gislason 2008; Robock et al. 2009; Duggen et al. 2010; Olgun et al. 2011; Kutterolf et al. 2013; Metzner et al. 2014).

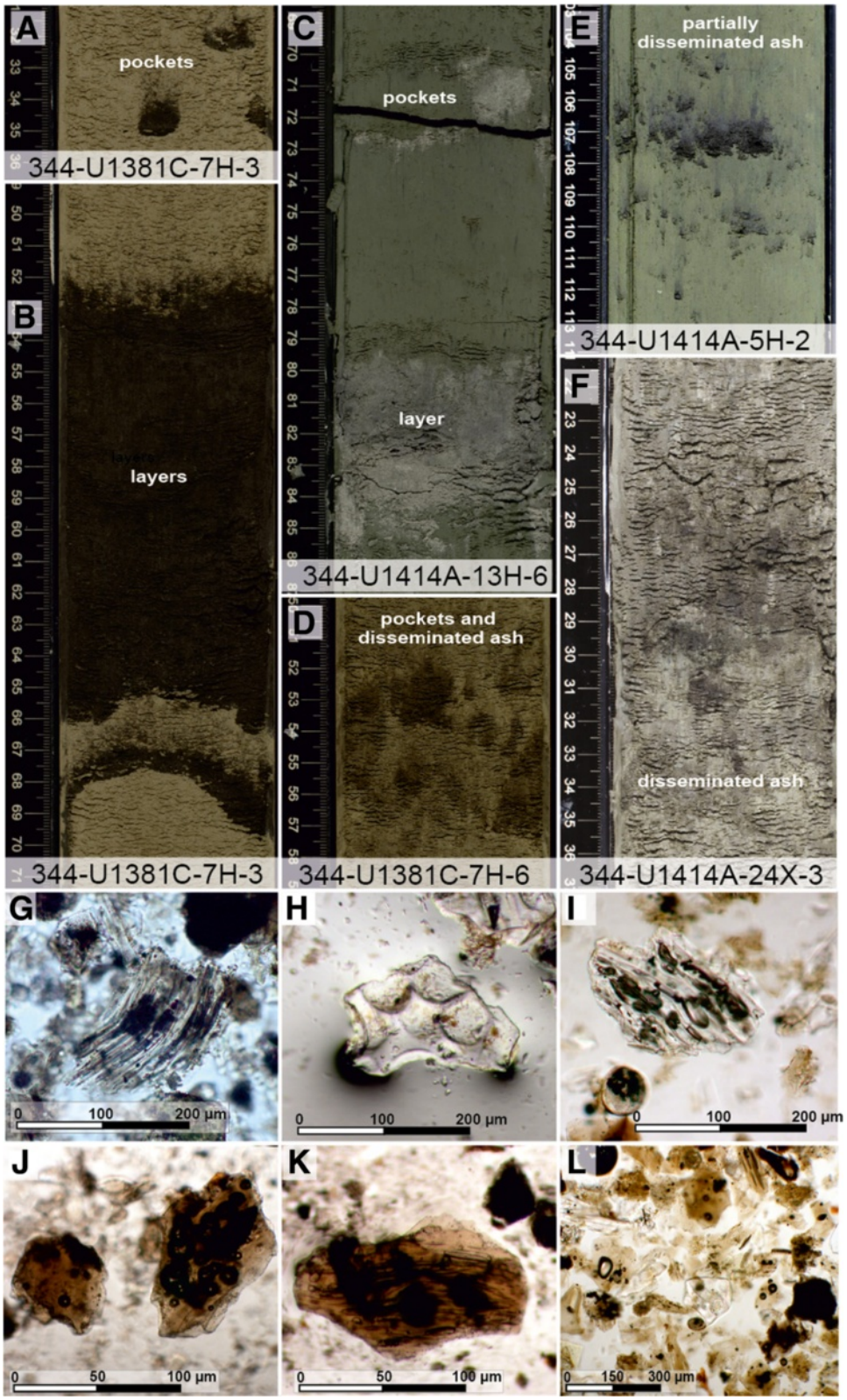

Fig. 2 (See legend on next page.)

(See figure on previous page.)
Fig. 2 Photographs of **a** mafic pockets, **b** discrete mafic ash layers, **c** felsic ash layer and pockets, **d** disseminated mafic ash pockets selected primary mafic ash layers, **e** partially disseminated ash pockets, and **f** disseminated ash. All examples from IODP expedition 344 (CRISP II) offshore Costa Rica. Example smear-slide microphotographs showing glass shard textures of felsic (G-I) and mafic (J-L) marine ash layers. **g** U1381-3H-7, 14–19 cm: felsic ash with tubular transparent to light brown shards. **h** M66-226/78 cm bsf: silicic shard from highly vesicular pumice. **i** M66-222/51 cm bsf: pumice fragment with moderately elongated vesicles. **j** M66-223/305 cm bsf: blocky sideromelane shard with and without vesicles. **k** M66-222/436-441 cm bsf: elongated vesicles in sideromelane shard. **l** M66-222/517–518 cm bsf: overview picture of different glass shards in one sample

Ash is commonly altered on and/or in the seafloor by diagenesis. In addition to the research cited above, for example, in a historically classic study, Gardner et al. (1986) observed many thin, pale green laminae (PGL) in the sediment cored during Deep Sea Drilling Project (DSDP) Leg 90 (Lord Howe Rise), which they identified as bentonites resulting from discrete ash fallout events. They found the temporal distribution of the PGLs to be similar to that of the discrete layers and logically concluded the PGLs were merely altered ash. For dispersed ash, however, the alteration increases the complexity for the application of techniques based on sedimentological and physical separation (e.g., grain size or sequential leachings to arrive at an aluminosilicate "residue"), because a fine-grained altered aluminosilicate ash is difficult to distinguish from, for example, fine-grained aluminosilicate eolian dust. The geochemical techniques summarized in this review, however, will still identify these alteration products as part of the original ash contribution to the sediment. For example, Hein et al. (1978) showed that ash beds in the Bering Sea become more altered with burial and form bentonite layers. They also documented that the chemistry of the bentonite beds reflects the chemistry of the parent ash, and differentiated authigenic smectite, which forms from the *in situ* breakdown of glass in ash layers or glass shards dispersed throughout the sediment, from detrital smectite derived from subaerial breakdown of recycled volcanic debris.

The use of tephra as a stratigraphic and chronologic tool has a long and wide-ranging history (e.g., Cambray et al. 1995; Straub and Schmincke 1998; Lowe 2011) and we do not intend here to repeat those efforts. Rather, in this paper, we (a) present a review of previous geochemical approaches to quantify dispersed ash in the Caribbean Sea and equatorial Pacific Ocean, (b) provide a summary of recent work applying a combined geochemical and multivariate statistical technique to identify dispersed ash in the northwest Pacific Ocean, and (c) describe preliminary results moving toward a regional assessment of inputs to the western Pacific Ocean (Fig. 1). We include some areas of research that are currently unresolved as they are likely to provide further insight into the nature and distribution of this important component of marine sediment. While radiogenic isotopes have proven helpful in studies of dispersed ash and the very fine detrital component (e.g., Ziegler et al. 2008; Scudder et al. 2014), in this paper we focus on major, trace, and rare earth elements since they are more commonly used in the various regions we discuss.

Review

Geochemical approaches: theory and practice

Composition is different from transport

A basic tenet of provenance research is that studies based on chemical, isotopic, or mineralogic composition, or many aspects of sedimentology (e.g., grain size), cannot alone infer the transport pathway (e.g., eolian vs. subaqueous transport) by which a grain of volcanic ash eventually becomes entrained in the sediment. Strictly speaking, transport pathway must be inferred based upon geological or geographic constraints. For example, in the context of eolian transport of eroded continental material, truly detrital aluminosilicate grains must be transported by wind to reach the deepest and most distal north Pacific (Rea and Leinen 1988; Kyte et al. 1993; Rea 1994).

For volcanic ash, however, the situation is more complicated. Subaqueous eruptions can lead to significant volcanic input (e.g., Fiske et al. 2001; Maicher and White 2001; White et al. 2003; Tani et al. 2008). Fiske et al. (2001, their p. 822) in particular note how the finest-grained fraction is missing from caldera deposits in the Izu-Bonin system. This "missing material" undoubtedly ends up as dispersed ash throughout the bulk sediment and due to its grain size has the potential to be advected great distances away from its point of origin. Determining this material's composition in the bulk sediment, a priori will not differentiate between subaerial (eolian) or subaqueous transport.

Subaqueous eruptions can also lead to pumice rafts, which may persist in the ocean for weeks, months, or years (Simkin and Fiske 1983; Risso et al. 2002; Bryan et al. 2004). Even in today's modern era of enhanced ocean and atmospheric observation, such occurrences are surprises (BBC News, 10 Aug. 2012). Yet, although these events may be uncommon on the human timescale, they are most likely significant pathways of ash to the deep sea over longer time frames.

Mixes of mixtures

In the broad context of geologic material, all non-biogenic rocks and sediments on the surface of Earth can be chemically described as falling along a mixing line or mixing curve between families of primordial materials (e.g., basalts) and families of fractionated "upper continental crust". Deviations from such a mixing line or curve are due to local provenance effects, authigenic/diagenetic resetting, weathering, and other processes, but the overall relationship holds true. While such a compositional range may seem relatively easy to differentiate analytically (e.g., felsic vs. mafic), the cases are rare when there are only two aluminosilicate sources and they are sufficiently compositionally distant from each other along the mixing line or curve. Far more common is the challenge of resolving multiple sources that are each at different fractional lengths along a theoretical mixing line or curve. For example, continental crust has been approximated as "granodiorite", "dacite", or other intermediate composition igneous/volcanic rocks (e.g., Taylor and McLennan 1985), and therefore distinguishing eroded continental crust from wind-blown dacitic ash is challenging. Or, still more challenging are scenarios whereby two disparate sources such as a marine basalt and a wind-blown dust of broad continental crust composition are both authigenically altered to, for example, assorted smectites, and thus have the potential to appear as a single source.

The above examples speak to the importance for geochemical studies of dispersed ash to address their attention to refractory elements that are appropriate to unravel mixing problems and that will also be relatively unaffected by diagenetic and authigenic processes. There are no chemical elements that unambiguously record any single geochemical provenance or domain. Within the spectrum of potential elements for use in general characterization as well as the multivariate statistics discussed below, inclusion of certain common major elements such as Al, Ti, and Fe, along with certain common trace elements such as La and Sc, proves to be beneficial. On a case-by-case basis, certain other key elements such as Th, Nb, and Cr can be advantageous as well (e.g., Plank 2005), although interpretations based on only a few elements are likely to be less representative than studies based on suites of many elements. However, common elements involved in reverse weathering reactions (e.g., Mg, Mackenzie and Garrels 1966; Presti and Michalopoulos 2008) should be avoided for such studies of provenance, given their labile behavior.

The contribution from geochemistry teamed with multivariate statistics

A variety of geochemical approaches can help resolve such mixing issues. In certain situations, such as in the Caribbean Sea example below, single element "normative calculations" (e.g., Leinen 1987) are sufficient, while in other cases multiple different analytical and/or computational approaches need to be simultaneously deployed to develop a more holistic understanding of the geochemical variability within datasets. We emphasize here a combined geochemical approach that generates a wide-ranging elemental suite that is examined with multivariate statistics.

The overall approach we summarize in this paper is based on Q-Mode Factor Analysis (QFA) and two forms of multiple linear regression, a Constrained Least Squares (CLS) technique and a Total Inversion (TI) technique (Pisias et al. 2013). The history of these techniques, as well as the specific MATLAB scripts to apply them to marine sediment chemistry (and recommendations for their use), are detailed in Pisias et al. (2013). The interested reader is also pointed toward previous papers by Dymond (1981), Leinen and Pisias (1984), Zhou and Kyte (1992), and Kyte et al. (1993). In our research group, we have successfully used these techniques in marine sediment from the Cariaco Basin, Arctic Ocean, equatorial Pacific, northwest Pacific Ocean, and South Pacific Gyre (Martinez et al. 2007, 2009, 2010; Ziegler and Murray 2007; Ziegler et al. 2007, 2008; Scudder et al. 2009, 2014; Dunlea et al. 2015a, b), demonstrating their utility throughout a variety of oceanic depositional regimes.

QFA is a terrific tool because—among other things—it is an "objective" technique (e.g., Leinen and Pisias 1984) that is minimally affected by inadvertent researcher bias. There are no inputs other than the data itself. It is limited, however, in many cases in that the resultant compositional factor scores may not be geologically reasonable or geologically precise enough across the spectrum of the wide element menus commonly generated in today's world of rapid geochemical analysis. Factor analysis is best used to help identify the number of independent components (also referred to as "end members") and their general composition, but not necessarily the extremely specific composition thereof. Therefore, one of the limitations of using QFA alone is that the user often cannot identify the specific geologic source(s) of the bulk sediment.

The number of end members necessary to best describe the variability of the dataset (that is, the number of factors indicated by the QFA) helps steer the CLS and TI multiple linear regressions. Specifically, in order to identify the exact sources identified by QFA, the CLS or TI linear regressions must be applied. In CLS and TI, the researcher inputs the composition of potential end members and mixes them until the best solution is reached (the differences between CLS and TI are detailed in Pisias et al. (2013)). Thus, we use the QFA to generate an objective "answer" as to the number of sources and their broad composition(s), and then the

CLS and/or TI, based on thoughtful selection of potential sources derived from knowledge of previous work and the local/regional geology, to generate the quantitative mix of specific sources. Libraries of potential end members are typically (a) constructed from the literature of all likely volcanic contributors (that is, individual papers about the geochemistry of particular volcano or region), (b) compiled from international global databases (e.g., EarthChem; http://earthchem.org), and/or (c) developed internally from the study's own data (e.g., using the composition of a discrete ash layer to assess whether it could potentially be a contributor to the dispersed ash component.).

Despite the quantitative attractiveness of applying statistical treatments to a well-measured geochemical dataset, there is no single diagnostic "magic bullet" to fulfill the task of identifying the dispersed ash component within bulk sediment. Instead, a series of interpretative techniques must be used prior to applying the statistical techniques. The use of standard geochemical approaches such as expressing data as concentrations, calculation of fluxes and/or elemental ratios, study of simple coefficient of determination (R^2) matrices, *x-y* diagrams, and other well-established approaches is extremely important. Such approaches define the boundaries for mass balance, allow comparison with lithologic descriptions and mineralogy, help ground the ensuing statistical treatments, and, in a way that is hard to quantify, ensure that the researcher is intimately familiar with the fundamental underpinnings of each dataset.

Finally, statistical treatments such as those discussed here often lead to non-unique solutions. Contextual oceanographic or geological knowledge plays a major role, however, and can eliminate some of the non-unique solutions. Our group takes a very labor-intensive approach to dealing with this broad subject for both factor analysis and multiple linear regression, strategically built around performing dozens to hundreds of statistical runs per dataset to assess sensitivity of, and variability in, the results (Scudder et al. 2009, 2014; Dunlea et al. 2015a,b). Each dataset is different, and we have found some in which any variation in one element will make a difference; but in another dataset varying a different element will exert a larger lever arm. We take great care to ensure that our results are not dependent upon, or unique to, one or two narrow statistical models nor to one or two specific elements. Doing so would be counter to the very nature of our task at hand—to develop a widely applicable, internally consistent understanding of "What is marine sediment made of?"

Previous work

In this section, we present a review of previously published studies focused on unraveling bulk marine sedimentary compositions. These case studies range from a simple three-component system (Caribbean Sea) in which element normative calculations alone are sufficient to determine the end members, to a very complex system in which the bulk sediment is composed entirely of aluminosilicates with very similar compositions that requires a combination of geochemical and statistical technique in order to identify the individual compositions (Izu-Bonin-Mariana Arc).

Caribbean sea: a simple case

The Caribbean Sea is ringed by volcanic arcs (Fig. 1; Sigurdsson 1999). To the west rises the Central American volcanic arc system, with a spectrum of volcanic edifices ranging in size from basaltic cinder cones to large stratovolcanos and calderas. To the east is the Antilles island arc, from which some of the most famous volcanic eruptions in the world originate (e.g., Lesser Antilles, Carey and Sigurdsson 1978). These combined volcanic systems contribute large amounts of ash to sediment in the Atlantic Ocean and Caribbean Sea from the Miocene on (Carey and Sigurdsson 1980, 2000; Peters et al. 2000; Jordan et al. 2006; Expedition 340 Scientists 2012; Le Friant et al. 2013) Ocean Drilling Program (ODP) Leg 165 cored throughout the Caribbean Sea (Fig. 1) with its most important objectives being related to the Cretaceous-Neogene bolide impact. One surprise that resulted from this research cruise was the startling number of discrete ash layers (Fig. 3, Carey and Sigurdsson 2000; Sigurdsson et al. 2000), their extent in time and space of which was unexpected. In addition to the discrete ash layers, shipboard study observed ash dispersed throughout the background sediment. Bulk chemical analyses of the bulk sediment allowed for the development of a single-element normative calculation scheme to quantify the abundance of this dispersed ash in these carbonate-rich sediments (Peters et al. 2000). Fortuitously, most of the sequence is a relatively simple three-component system (of $CaCO_3$, terrigenous, and ash), which facilitated the study of dispersed ash in parallel to the discrete layers. Petrographically, the bulk sediment appeared to consist of only carbonate and aluminosilicate clay—and the aluminosilicate clay was assumed to be entirely comprised of eroded terrigenous material (Peters et al. 2000).

Bulk chemical analyses, however, demonstrated that the sediment was vastly depleted in Cr beyond that, which could be explained by carbonate dilution. For example, in a sample with an equal (50 and 50 %) mix of $CaCO_3$ and terrigenous clay, one would predict there should be ~55 ppm Cr in the bulk composition (based on typical "average shale" of ~ 110 ppm Cr, using Post-Archean average Australian Shale [PAAS] from Taylor and McLennan (1985) to broadly represent an upper crustal terrigenous source). However, such a sample would instead present <10 ppm Cr, indicating that the brown aluminosilicate

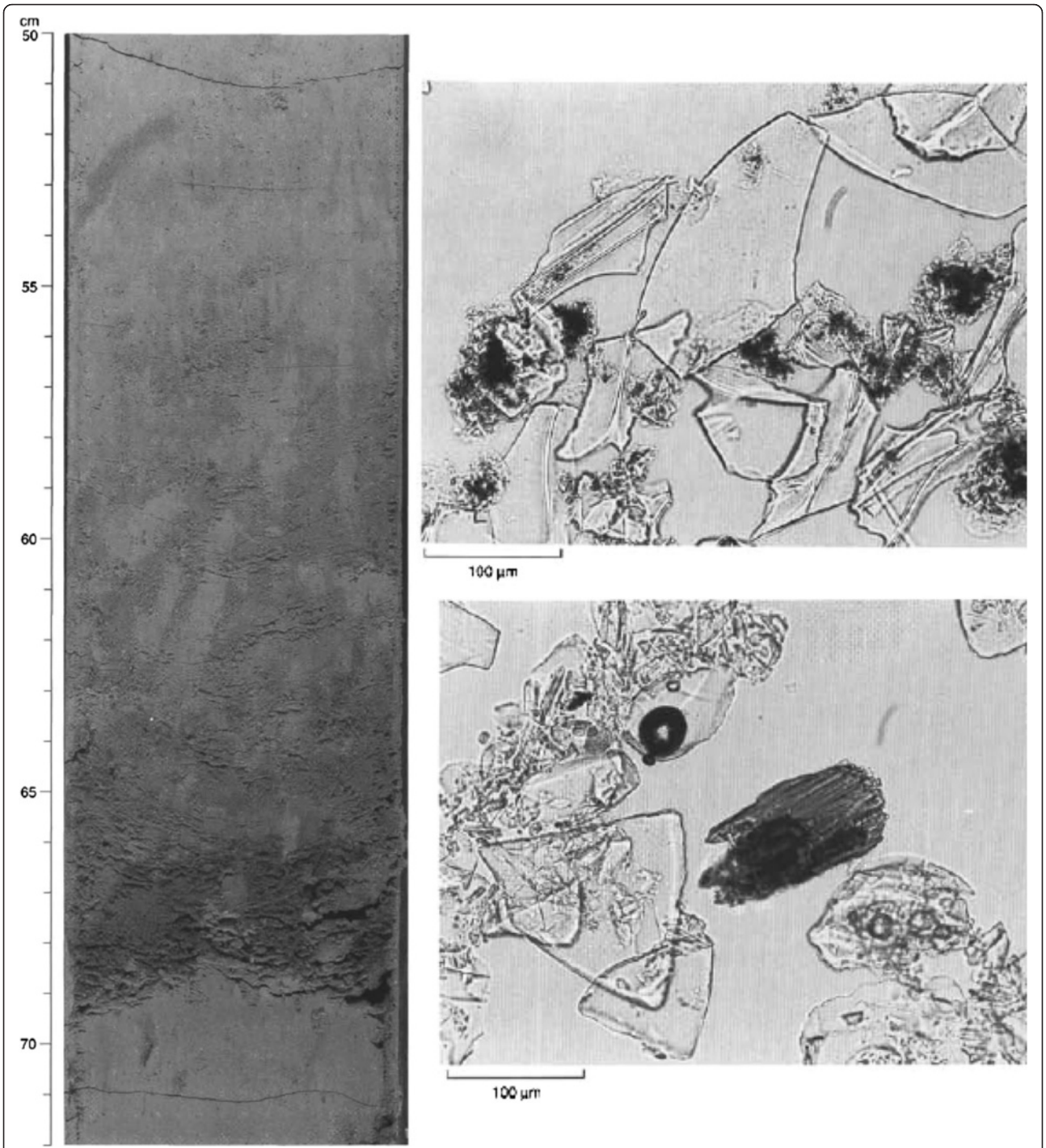

Fig. 3 Closeup photos and photomicrographs of ash layers from ODP Site 998, western Caribbean Sea. *(Left)* Volcanic ash layer in Section 165-998A-10H-4, 50–72 cm. Note the sharp base and transitional top that has been reworked by bioturbation. *(Right, top)* Section 165-998A-19X-3, 55–56 cm. Typical rhyolitic glass shards from a 13.8 Ma volcanic ash fall layer. The width of the field of view is 0.5 mm. *(Right, bottom)* Typical fresh (*clear*) and altered (*cloudy*) glass shards and an amphibole phenocryst in a 15 Ma volcanic ash fall layer in Section 165-998A-21X-3, 51–52 cm. From Sigurdsson, Leckie, Acton, et al. 1997

groundmass was not solely detrital terrigenous material (Peters et al. 2000).

Given the simple three-component system, normative calculations (Leinen 1987) were appropriate to identify the sources to the bulk sediment. Peters et al. (2000) based their calculations on Cr, given that the end member values of Cr in typical shale (110 ppm) and rhyolite (<3 ppm) are strongly divergent. Thus, in a

three-component system of $CaCO_3$ (which is quantified precisely by coulometry), terrigenous material (calculated via Cr), and ash, the amount of ash can be calculated by difference, as follows:

$$(\%\,\mathrm{Ash})_{\mathrm{sample}} = 100 - (\%\ \mathrm{CaCO_3})_{\mathrm{sample}} - (\%\ \mathrm{Terrigenous})_{\mathrm{sample}}$$

where

$$(\%\,\mathrm{Terrigenous})_{\mathrm{sample}} = 100 * \left(\mathrm{Cr_{sample}}/\mathrm{Cr_{PAAS}}\right)$$

Peters et al. (2000) thus documented on a sample-by-sample basis that dispersed ash comprises 15–20 wt.%, with a maximum of 45 wt.%, of the bulk sediment in the western Caribbean. These values were consistent with the sedimentological smear-slide analyses (Sigurdsson et al. 1997) but were more precise.

Peters et al. (2000) also observed that the timing of the accumulation rate of dispersed ash paralleled the sedimentation rate of the discrete layers, although the maxima in dispersed ash preceded the Miocene and Eocene maxima in discrete layers by ~2–4 Ma (Fig. 4). They interpreted the relative timing as recording arc evolution, with the dispersed ash being generated by smaller volcanoes characteristic of the more juvenile arc, and the larger discrete layers representing a mature arc characterized by larger stratovolcanoes and caldera

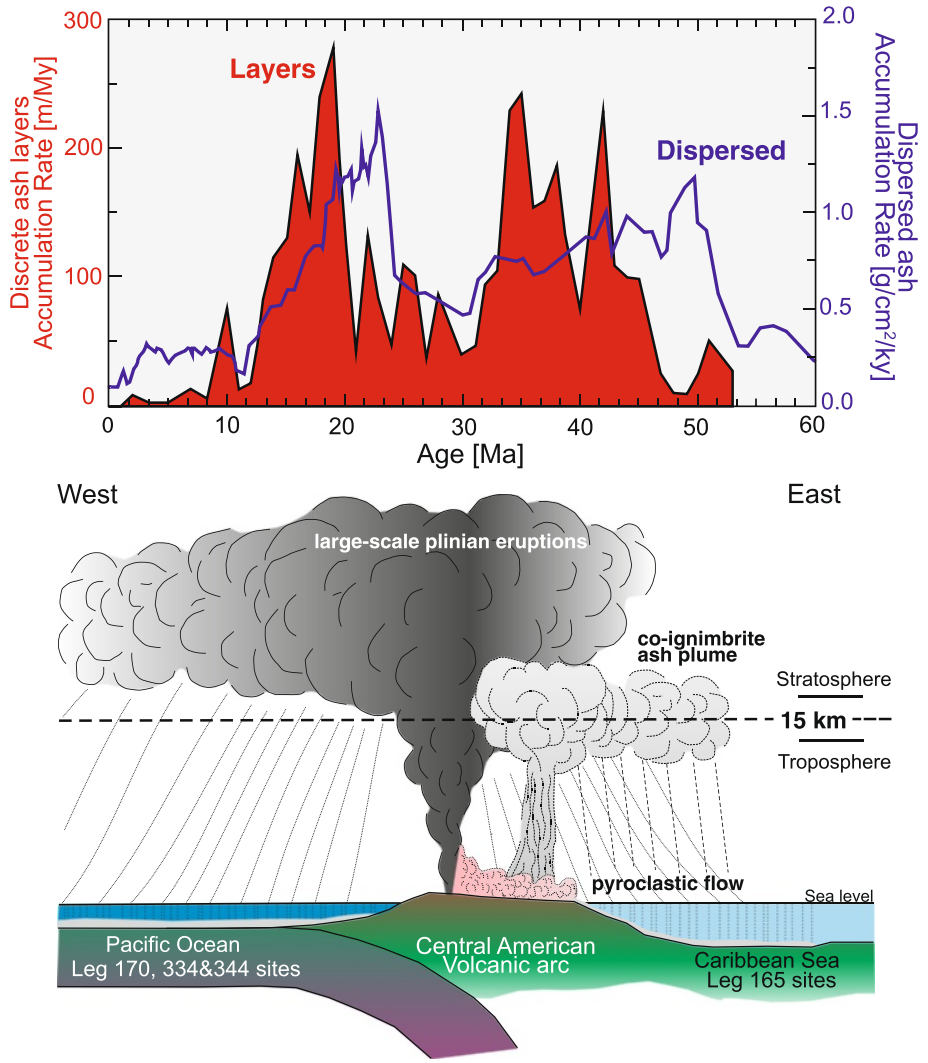

Fig. 4 (*Top*) Dispersed (*blue line*) vs. discrete (*red field*) ash accumulation in the Caribbean Sea. Accumulation of discrete ash layers (Carey and Sigurdsson 2000; Sigurdsson et al. 2000) and dispersed ash (Peters et al. 2000). ODP Site 998, western Caribbean Sea. (*Bottom*) Eruption transport and deposition patterns for recent to Miocene eruptions of the Central American Arc. Large plinian eruption columns (*light to dark gray*) reach deep into the stratosphere and are therefore transported to the west by the prevailing winds. Large ignimbrite-generating eruptions, predominantly in the Miocene, generate co-ignimbrite ash plumes (*pinkish to light gray*) reaching only into the upper troposphere/lower stratosphere and are therefore distributed to the east. Tropopause is shown with a *dashed line* at 15 km altitude. *Gray fields* below the sea level demonstrate submarine ash deposits

systems, as suggested by Carey and Sigurdsson (2000) and Sigurdsson et al. (2000). These are capable of injecting large plumes of Central American co-ignimbrite ash into the lower stratosphere and upper troposphere, that is, the ideal atmospheric height to facilitate west-to-east blowing wind transport (e.g., rather than transport from east-to-west in the higher stratosphere) (Fig. 4). This interpretation is consistent with the previous studies that have shown that Paleogene and Neogene Central American volcanism is predominantly characterized by larger ignimbrite-forming eruptions (Jordan et al. 2006) that may have frequently produced co-ignimbrite ash plumes reaching lower stratospheric heights (~15 to 20 km; e.g., Woods and Wohletz 1991; Bursik 2001), in contrast to the higher stratospheric eruption columns of Plinian eruptions (>>20 km; e.g., Kutterolf et al. 2008a).

Equatorial pacific ocean: a complex case

Our group also has a long-standing interest studying the equatorial Pacific (e.g., Murray and Leinen 1993, 1996; Murray et al. 1993, 1995, 2000; Kryc et al. 2003; Ziegler and Murray 2007; Ziegler et al. 2007, 2008, plus others). The non-biogenic component of these sediments includes terrigenous clay and ash, which are challenging to resolve in sediment with more than 98 % biogenic material (carbonate and biogenic silica). Some of our work specifically targeted how to resolve the eolian, ash, and authigenic components of these sediments and built upon the classic research of the long-standing Michigan group and their progeny (e.g., Hovan et al. 1991; Rea 1994; Rea et al. 1998).

For example, Ziegler et al. (2007) detailed chemical criteria that can be applied to differentiate authigenic, terrigenous, and volcanogenic aluminosilicates from each other. Sequential extractions were performed at ODP Site 1215 (Fig. 1) to remove non-aluminosilicate components. The material remaining upon completion of the extraction procedure was termed the "residual" component, consistent with established protocols. La-Sc-Th ternary diagrams and PAAS-normalized rare earth element (REE) patterns (Fig. 5a) and reference REE patterns (Fig. 5b) were used to aid in determination of the sedimentary components. In the residual component, Ziegler et al. (2007) quantified upper continental and lower crustal components using selected rare earth element (REE), Sc, and Th abundances. In old (>50 Ma) nannofossil ooze, the residual component exhibited a large La contribution. Additionally, the residual component of the nannofossil ooze fell outside the boundaries of a simple two component mixing between upper and lower crust components. REE patterns for these samples exhibit sharp, seawater-like negative Ce anomalies, providing a clear indication that an authigenic phase is present in the residual component (Fig. 5c). The old age of these sediments may contribute to the formation of the authigenic phase, given that such samples have likely experienced significant diagenesis. In this way, the geochemical approach clearly identified samples in which it is virtually impossible to differentiate eolian material from volcanic ash (Fig. 5c, d).

Izu-Bonin-Mariana Arc (ODP Site 1149 and DSDP Site 52)

One of the goals of ODP Leg 185 was to test whether subducted sediments control along-strike geochemical differences in Izu-Bonin-Mariana arc composition (Fig. 1, Plank et al. 2000). In addition to the potential influence of the terrigenous (non-ash) sedimentary component, the amount of ash in the sediment column is critical to constrain, not only for the determination of absolute geochemical fluxes into the "Subduction Factory" but also in order to determine how much of the input is "recycled" from the arc itself. Due to the long-standing interest in the region from a variety of geological perspectives, there is also a wealth of tectonic- and arc-related information to draw upon in the context of both ash layers and dispersed ash.

Preliminary work based on a Nb-based normative calculation showed that 33 ± 9 wt.% of the sediment at ODP Site 1149 is comprised of dispersed ash (Plank et al. 2000). As described in Scudder et al. (2009, 2014), in order to determine the sources to the bulk sediment, we followed the QFA and TI approaches and MATLAB scripts from Pisias et al. (2013). The elemental suite we targeted was composed of refractory elements predominantly associated with aluminosilicate components (Al, Ti, Sc, Cr, Ni, Nb, La, Th) as these are the most likely to identify differences between source components. The QFA results indicate that four factors (end members) explain 97 % of the variability of the bulk sediment (Scudder et al. 2014, Fig. 6). Given that QFA alone is not sufficient to identify the source of these factors, TI modeling was employed. The TI modeling identifies a combination of Chinese Loess (CL), rhyolitic ash from the Honshu arc (HR), mafic ash from the Izu-Bonin Front Arc (IBFA), and a second eolian dust (termed "Eolian 2") that best explain the total chemical composition of the bulk sediment.

Based on the TI results, the dispersed ash mass accumulation rate (MAR, g/cm^2/ky) at Site 1149 can be calculated and compared to the MAR of a series of ash layer parameters. At this site, the number of ash layers most closely tracks the total dispersed MAR (that is the sum of HR + IBFA). That the number of layers is most similar to the dispersed MAR suggests that eruption *frequency*, rather than eruption *size*, is the driving mechanism for the dispersed ash record (Scudder et al. 2014, Fig. 7).

The MAR patterns of the ash components are consistent with published eruption records of both the

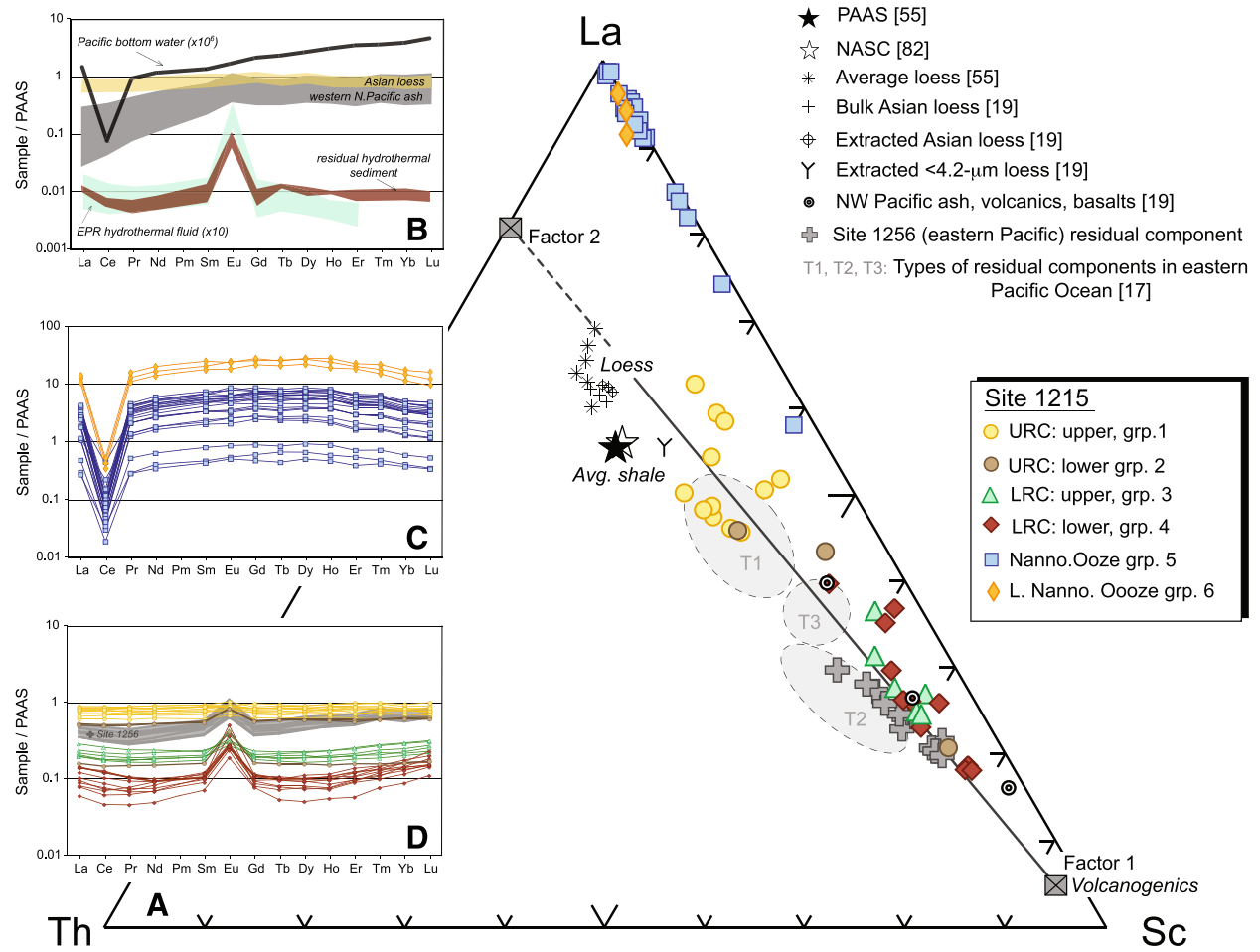

Fig. 5 **a** La-Sc-Th ternary diagram and PAAS-normalized rare earth element (REE) patterns from Site 1215 (central Pacific) and Site 1256 (eastern Pacific) from Ziegler et al (2007). **b** Reference REE patterns. Asian loess (Jahn et al. 2001), western Pacific ash (Bailey 1993), EPR and Pacific bottom water (Piepgras and Jacobsen 1992), hydrothermal residual sediment (Severmann et al. 2004), and hydrothermal fluid (Klinkhammer et al. 1994). **c** Residual component extracted from early-mid Eocene biogenic sediment at Site 1215 as defined in Ziegler et al. (2007). Note the significantly negative Ce anomaly indicating a seawater source. **d** Residual component extracted from the red clay unit from Site 1215 and the silty nannofossil ooze from Site 1256 as defined in Ziegler et al. (2007). See legend for symbol description. Groupings are based on REE patterns. Factor 1 is interpreted as lower crust island arc volcanic arc material and Factor 2 is similar to upper continental crust. T1, T2, and T3 are eolian dust samples classified based on REE patterns, Eu/Sm, and La/Sc ratios from Hyeong et al. (2005). *URC* upper red clay; *LRC* lower red clay

Izu-Bonin and Honshu arcs, and we can interpret these changes in accumulation rate in terms of arc history (Fig. 8). Focusing first on the Honshu Rhyolite, we observe that this component is the dominant dispersed ash, even though the Honshu arc is relatively far away. Given Site 1149's distal location, eruptions from the Honshu arc could have been large and yet resulted in only thin layers. These layers may subsequently be mixed into the bulk sediment to create the dispersed ash component. Alternately, the dispersed ash could simply represent an increase in deposition of ash from the atmosphere. The MAR of HR is consistent with the tectonic history of the Honshu arc, particularly through the younger portions of the record (e.g., Taira 2001). For the IBFA component, the models closely track the temporal changes in the tectonic record of Izu-Bonin (e.g., Sibuet et al. 1987). MAR patterns indicate that a gradual increase in IBFA volcanism occurred from ~18–10 Ma, with a burst of activity from ~4.5–3 Ma followed by a steady increase beginning at ~2 Ma (Scudder et al. 2014, Fig. 8).

We can compare and contrast Site 1149 to DSDP Site 52 in the northern Marianas arc (Fig. 1). Site 52 contains extremely high abundances of volcanic ash not directly linked to a specific eruption style (upwards of 50 % volcanic glass mixed in the brown clay; Fischer et al. 1971). Unfortunately, rotary drilling at Site 52 left only a few ash layers intact (all in the upper 20 mbsf; Fischer et al. 1971). Applying QFA with the same chemical suite as used at Site 1149 indicates that four factors (end

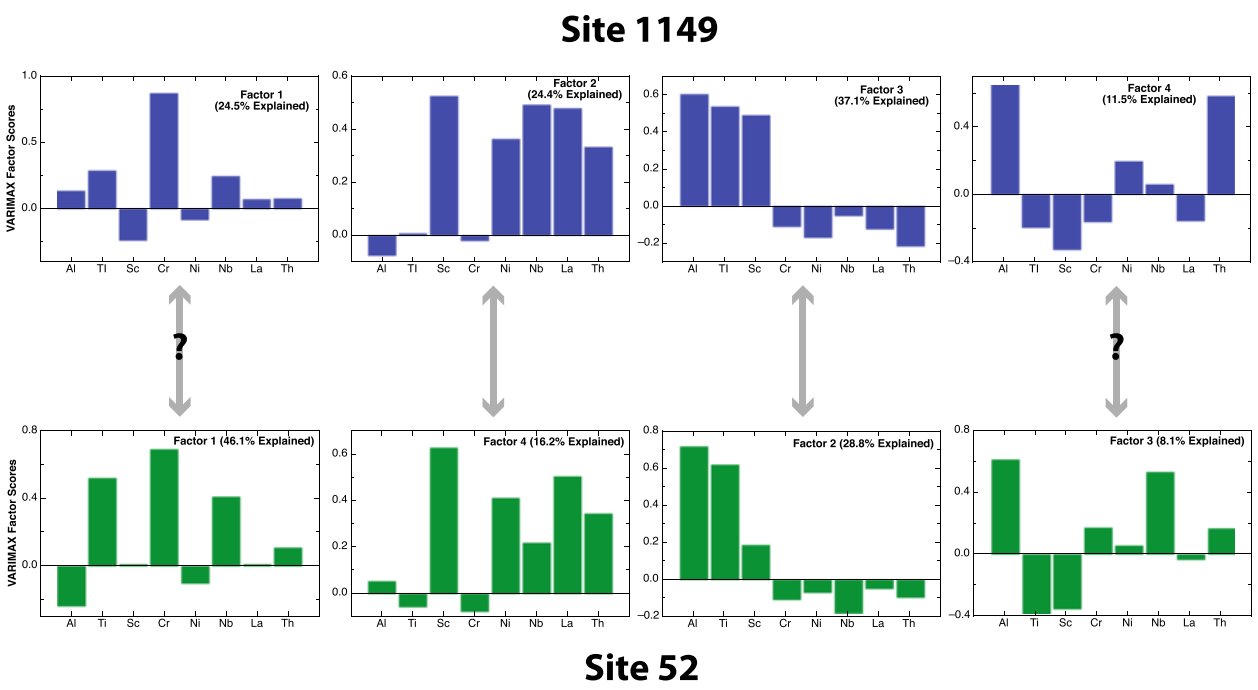

Fig. 6 VARIMAX factor scores from QFA, *(Top)* Site 1149, *(Bottom)* Site 52, from Scudder et al. (2014). Note the similarities between Site 1149 Factor 2 and Site 52 Factor 4 as well as Site 1149 Factor 3 and Site 52 Factor 2

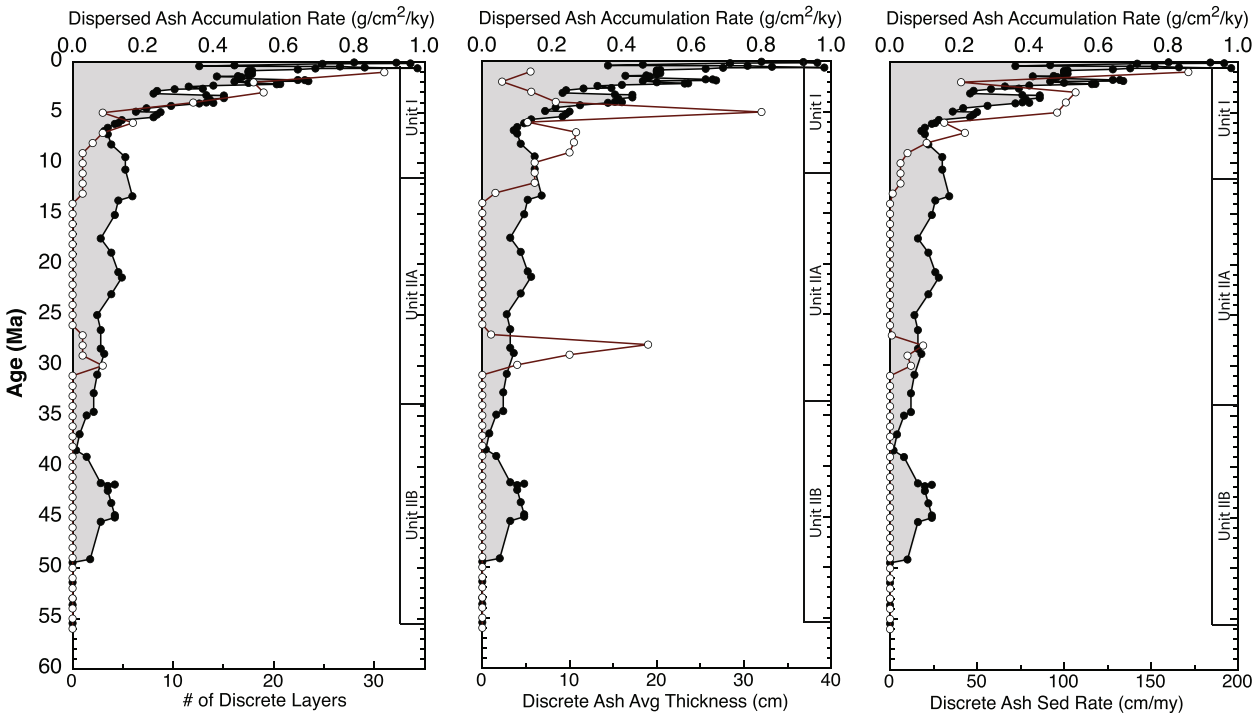

Fig. 7 Site 1149. The accumulation rate of total dispersed ash (*gray shaded* with *filled circles* in g/cm^2/ky) plotted against parameters associated with the sedimentation of discrete ash layers per 1 Ma (*open circles*) from Scudder et al. (2014)

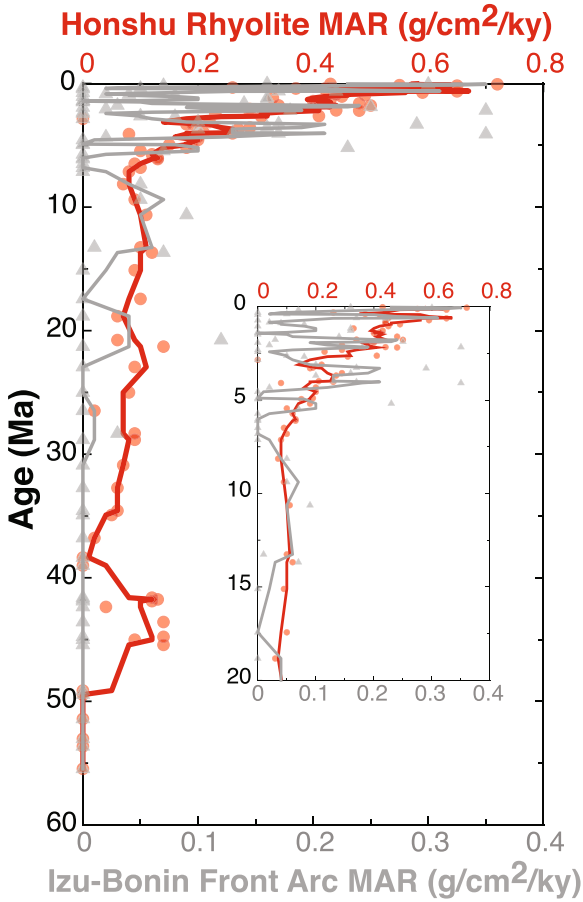

Fig. 8 Individual data and three-point averages of MARs of each dispersed ash end member, Site 1149. *Inset* focuses on the younger portion of each record. Note color-coded different *x*-axis scales and labels. From Scudder et al. (2014)

members) are present (Fig. 6). Two of these factors closely resemble those found at Site 1149, while the other two do not correspond well, if at all (Scudder et al. 2014). Given the limitations of QFA described previously, this interpretation is based on the factor scores (the weight of each element on the discrimination of a single factor) and the broad compositional scores produced by the modeling. TI linear modeling confirms this interpretation, identifying a mix of Chinese Loess, IBFA, dispersed boninite from the Izu-Bonin arc (BNN), and a dispersed felsic ash with the same composition as felsic layers from Site 52 (referred to as Felsic52) as best explaining the bulk sediment chemical composition.

Site 52 presents some key similarities and differences from Site 1149. First, the total amount of dispersed ash (regardless of composition) at both sites is very high, averaging 30 ± 17 wt.% at Site 1149 and 36 ± 18 wt.% at Site 52. Second, whereas at Site 1149 the two ash sources (HR, IBFA) are found both as layers and as dispersed ash, at Site 52 at least three volcanic sources are required to explain the bulk composition of the sediment. The discrete layers appear to be IBFA and felsic ash layers from Site 52, while the dispersed ash is comprised of IBFA, Felsic52, and an additional component, average Izu-Bonin Boninite (BNN). Therefore, at Site 52, the ash layers and the dispersed ash are partially compositionally decoupled from each other (Scudder et al. 2014).

Ongoing research

In this section, we present new data and ongoing observations from a variety of settings in the Northwest Pacific. While some of this research may still be developing, we include it here in order to show the strength of the combined geochemical/statistical technique in moving toward a regional perspective of inputs to the Western Pacific.

Nankai Trough, IODP Sites C0011 and C0012

IODP Sites C0011 and C0012 (Fig. 1), drilled as part of the Integrated Ocean Drilling Program (IODP) NanTroSEIZE transect, are located in the Shikoku Basin ~ 100 km southeast of the Kii Peninsula and ~160 km west of the Izu-Bonin arc on the Kashinosaki Knoll, a prominent bathymetric high. Located near the crest of the Kashinosaki Knoll, Site C0012 represents a condensed sediment section in comparison to Site C0011, which is located on the northwestern flank. The main goal of NanTroSEIZE is to drill across the up-dip limit of the seismogenic and tsunamigenic zone over the Nankai Trough subduction boundary, along which mega-thrust earthquakes are known to occur (Tobin and Kinoshita 2006). Shipboard sedimentological smear slide analyses at both Sites C0011 and C0012 estimate that on average dispersed ash constitutes ~ 25–30 wt.% through Units I and II, and decreases to ~7–15 wt.% in the hemipelagic facies of Unit III (Saito et al. 2010; Henry et al. 2012).

Statistical analyses of newly acquired data from Sites C0011 and C0012 were performed using the same element suite as that applied to Site 1149. At Site C0011, QFA indicates that three factors explain 99 % of the variability of the bulk sediment (Fig. 9). While we cannot determine the exact composition of the end members from QFA, one of the modeled sources appears to be intermediate (roughly equal contributions of most of the elements in the model, that is, of Sc, Cr, Ni, Nb, La, and Th) in composition while the other two are broadly felsic (contributions driven by Al, Ti, and Sc, with lesser covarying Nb, La, and Th). CLS multiple linear regression analysis suggest that the three sources at Site C0011 are consistent with one being PAAS, and the other two being ashes having compositions similar to a

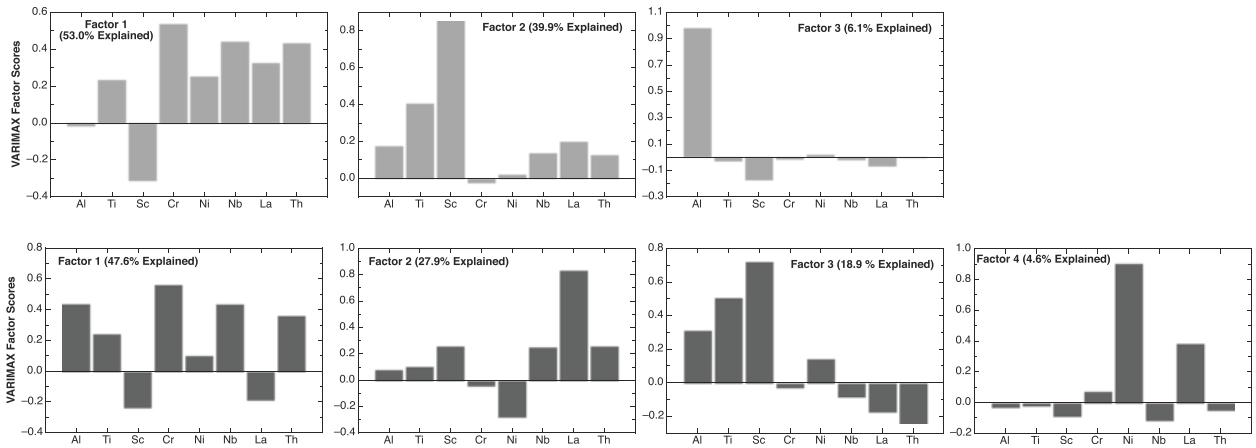

Fig. 9 VARIMAX factor scores from QFA. (*Top*) Site C0011. (*Bottom*) Site C0012

representative Rhyo-Dacite and Rhyolite from the Honshu Arc (HR) (Fig. 10). These latter two sources may in fact be dispersed ash but could also be ash that has since been altered and yet retained its refractory chemical signature. Regardless, these two types of dispersed ash and/or clay minerals with comparable geochemical signatures comprise 36 ± 8 wt.% of the bulk sediment. Evidence for multiple sources of volcanic material, and/or the chemically equivalent clay-alteration products, is consistent with studies of tuffaceous and volcaniclastic sandstones from this site, which calls for volcanic material from both the Izu-Bonin and Honshu Arcs (e.g., Pickering et al. 2013; Schindlbeck et al. 2013; Kutterolf et al. 2014).

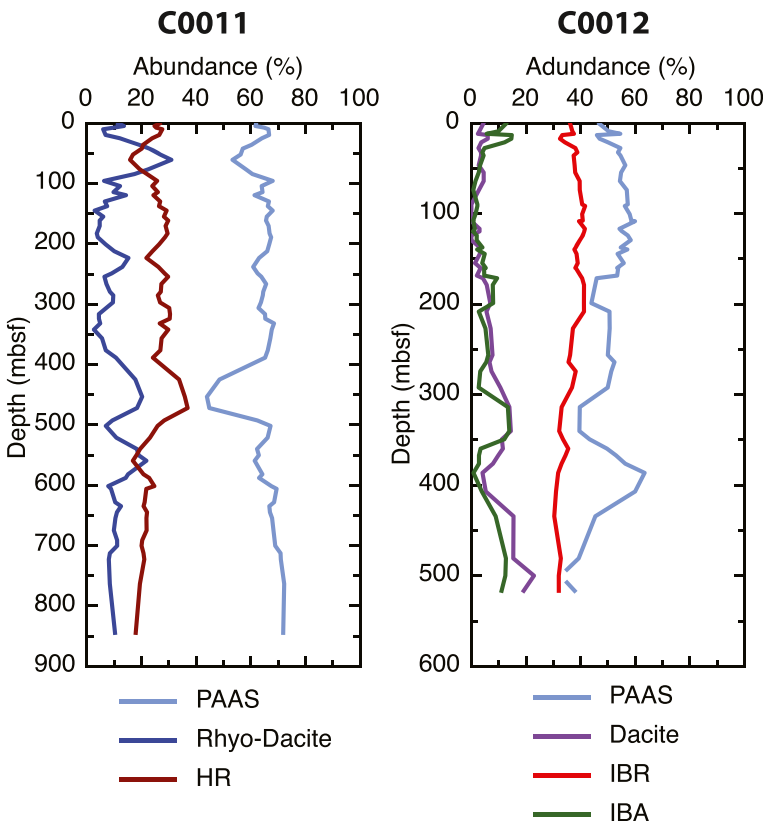

Fig. 10 Abundance (weight %) of sources identified by constrained least squares multiple linear regressions (CLS). (*Left*) Site C0011. (*Right*) Site C0012

Applying the same methods to Site C0012, QFA indicates that four factors (end members) explain 99 % of the variability in the bulk sediment (Fig. 9). The modeled compositions of the bulk sediment at Site C0012 identify two intermediate and two felsic end members for the geochemical proxies. CLS indicates that these end members are best explained by mixing PAAS and three ashes: the dacitic ash layers from Site C0012, rhyolite from the Izu-Bonin Arc (IBR), and andesite from the Izu-Bonin Arc (IBA). Collectively, the ash compositions (and/or their chemically equivalent clay-mineral alteration products) contribute approximately one-half (49 ± 10 wt.%) of the bulk sediment (Fig. 10). Here, it is important to recall that our geochemical approach cannot resolve the pathway by which the ashes have reached these sites, as some of these ashes may be eroded from terrestrial deposits in the Japanese archipelago.

We compare the mass accumulation rate of the dispersed ash (or its clay alteration) component to a number of common ash layer parameters, including the number of ash layers per 0.2 Ma, the thickest ash layer per 0.2 Ma, and the total thickness of ash layers per 0.2 Ma. We binned the data by 0.2 Ma units, in order to generate a discrete ash layer dataset of approximately the same temporal resolution as that of our dispersed ash record (Fig. 11).

When compared to various ash layer parameters, we find that the MAR of the total dispersed ash component at Site C0011 correlates best with "Thickest Layer" in Unit I. This suggests that through this interval, eruption volume, rather than the frequency of explosive eruptions, drives the dispersed ash accumulation (Fig. 11). In contrast, in Unit I of Site C0012, the number of discrete ash layers rather than "thickness" is best correlated to the dispersed ash MAR. At both sites, the number and thickness of ash layers vastly decreases below the Unit I/II boundary while the dispersed ash component remains high as a geochemical proxy. This is reflective of time periods when the volcanism in SW Japan was reduced or eliminated (Mahony et al. 2011), when the sites were influenced by siliciclastic turbidites (Units II, IV, and V), or when dispersal paths from the main detrital sources were further away from eruptive fronts (Unit III). Changes in any of these factors may have resulted in either fewer and/or thinner layers that would be more susceptible to being homogenized (by bioturbation or otherwise). That the geochemical signature equivalent to dispersed ash is high at times when so few ash layers were deposited clearly demonstrates that clay minerals derived from volcanic ash and volcanic rock (e.g., smectite group) are a much greater contributor to the sedimentary sequence than is recorded only by the ash layers.

Shikoku Basin, DSDP Site 444

DSDP Site 444 was drilled during Leg 58 to test hypotheses about the origin of marginal basins (Fig. 1, deVries Klein and Kobayashi 1980; deVries Klein et al. 1980). In particular, the Shikoku Basin portion of Leg 58 was drilled in order to answer questions regarding the basin formation by evaluating various spreading models, the ages of the oceanic crust, sediment evolution, and the paleoceanographic origin of the region (deVries and Kobayashi 1980). Site 444 was selected for our research on dispersed ash because of its abundant volcanic ash layers (for example, in comparison to Sites 442 and 443).

Site 444 contains basaltic, andesitic, and rhyolitic ash (deVries and Kobayashi 1980; Furuta and Arai 1980; and our own studies). Most tephra in other northwestern Pacific DSDP holes are rhyolitic and andesitic, which makes the basaltic nature of the Site 444 tephra geologically and tectonically unusual (White et al. 1980). In the Pleistocene and Pliocene, the ash layers are non-alkali rhyolites. As felsic ash is believed to mainly be a product of explosive volcanic eruptions, these layers could have originated from relatively large-scale eruptions in an island arc setting, most likely located westward of Site 444 and transported in the prevailing westerlies. This direction of transport is evident as grain size increases toward the west and decreases toward the east (Furuta and Arai 1980).

In the Miocene, the tephra is of non-alkali tholeiitic basaltic as well as alkali basaltic composition. These basaltic layers imply that another volcanic source was involved in the Miocene. This source could have been closer to the drilling sites than those sources of rhyolitic and andesitic tephra (possibly the Kinan Seamounts and the Shichito-Iwo Jima volcanic arc), but it could also be the distal evidence for large mafic eruptions from a more oceanic arc source. The knowledge that the occurrence of such large mafic plinian eruptions with a wide dispersion is not limited to arc settings alone and can also be found at ocean island settings (e.g., the Galápagos archipelago, Schindlbeck et al. 2015). Such observations are especially important for future studies of dispersed mafic ash in marine sediments. We note, however, that at least some of these ashes may also be subaqueous in origin. For example, certain volcanic arcs near the Shikoku basin (e.g., Izu-Bonin) contain subaqueous volcanoes (Hochstaedter et al. 2001).

Ash layers were carefully identified throughout the 310 meters of sediment at Site 444 using core photos and the shipboard lithologic description (deVries and Kobayashi 1980). Site 444 was cored using the Rotary Core Barrel (RCB) system, as it was occupied during the early-mid stages of the DSDP prior to the advent of the advanced piston corer. Because of the RCB drilling, the

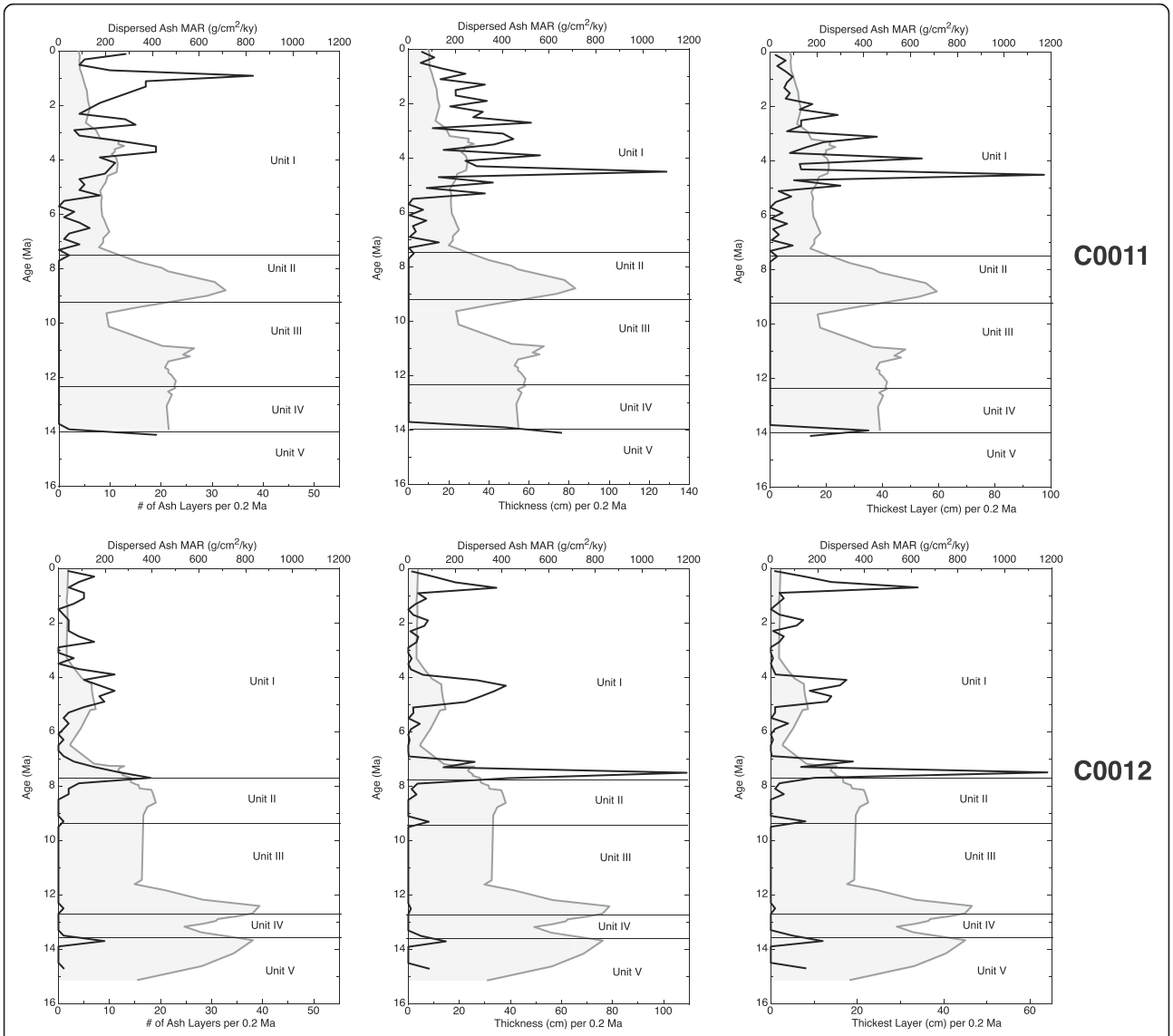

Fig. 11 The accumulation rate of total dispersed ash (*gray shaded line*, g/cm^2/ky, the same in each panel by site) plotted against parameters associated with the sedimentation of discrete ash layers per 0.2 Ma (*black line*, parameters are different in each panel as shown in the *bottom x*-axis labels). A moving 0.2 Ma window was chosen to bin each discrete ash layer parameter to approximate the resolution of the modeled dispersed ash record. (*Top*) Site C0011. (*Bottom*) Site C0012

recovered core is highly disturbed. Therefore, we classified the ash deposits as either an "ash layer" or an "ash pocket". Anything that is ash in distinct form but that is not in the shape of a full horizontal layer (e.g., touching both sides of the core liner) is termed an "ash pocket". The pockets are often, though not always, circular in form. Ash layers and ash pockets correlate with each other with depth. Thus, we interpret that the pockets are likely to have originated from ash layers mixed by RCB drilling.

A total of 128 ash layers and 76 ash pockets were identified. Of the 28 ash layers chemically analyzed in this study, four (4) of them are categorized as ash pockets. This is important to note when assessing their compositions as any seemingly unusual compositions can be evaluated for mixing with non-ash sources (e.g., clays). The distribution of ash layers and pockets were parameterized by (1) thickness with depth, (2) number of layers per 10 meters, (3) thickest layer (cm) over successive 10 meter depth increments, and (4) total thickness of ash (cm) in that same 10 meter window (Fig. 12). These parameters collectively should yield a baseline understanding of the distribution of ash layers, and we acknowledge that any one of these parameters is not necessarily preferable to the others. Additionally, we note that there is a relatively thick 31-centimeter-thick ash

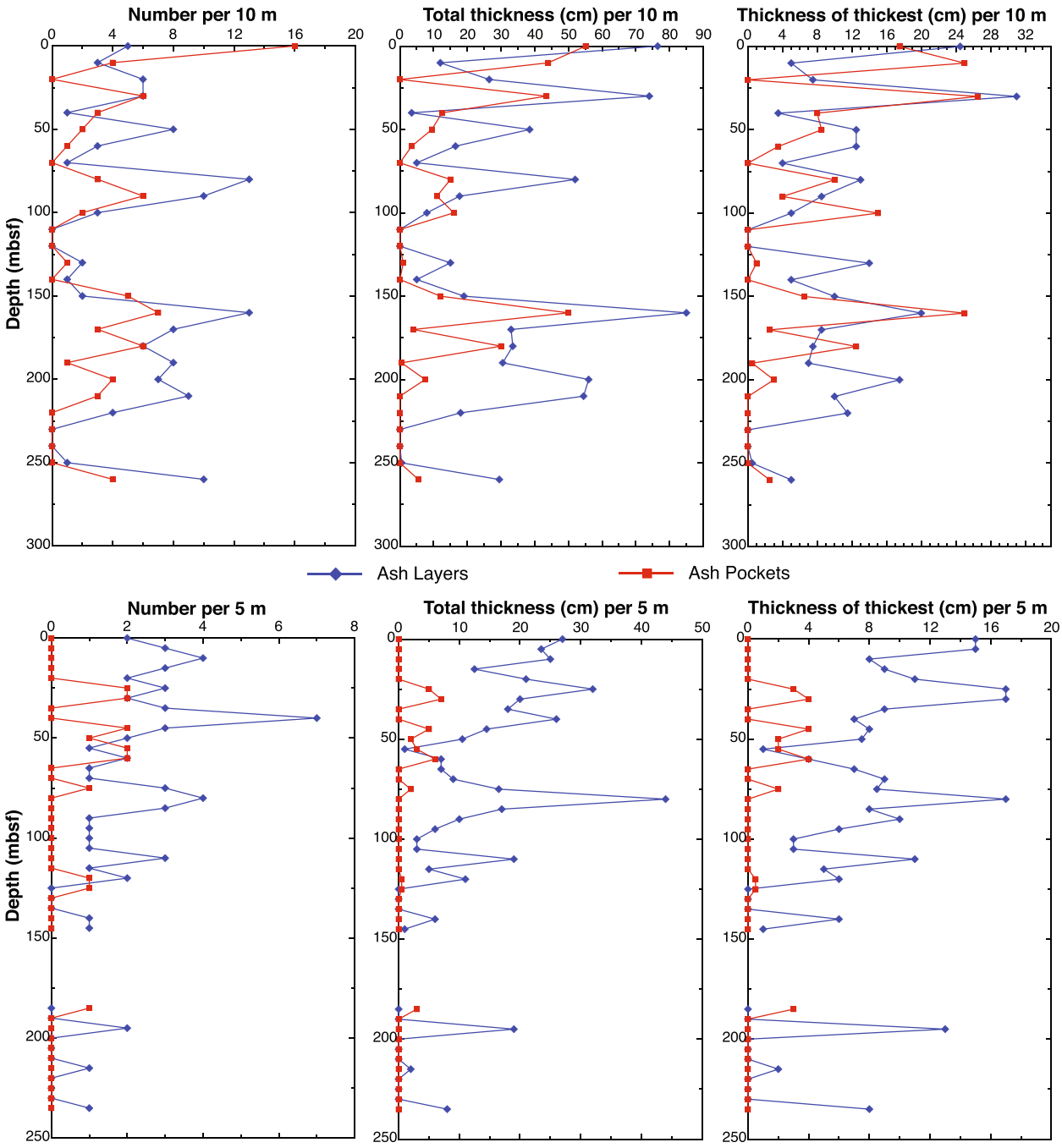

Fig. 12 Ash layer parameters, number of ash layers, total ash thickness (cm), thickness of thickest layer (cm). (*Top*) Site 444. (*Bottom*) Site 579/581

layer at a depth of 30 mbsf (~0.66 Ma, Pleistocene), which may overly influence some of these parameters over that interval.

Ash layers were analyzed for major element glass shard compositions by electron microprobe (average of 15 single shard measurements), and additionally, the bulk ash layers were analyzed by ICP-ES and ICP-MS for major, trace, and REE compositions following the methods of Scudder et al. (2014). Even though the bulk ash data may be compromised by the inclusion of the terrigenous aluminosilicate material (e.g., adjacent pelagic clay mixed into the ash layer or ash pocket; Scudder et al. 2014), we can still infer other key aspects of the distribution of the ash layer/pocket chemistry.

The distribution of key major elements used to differentiate compositional variation, such as SiO_2 or TiO_2, (Fig. 13), suggests the presence of multiple ash populations

ranging from mafic to intermediate to felsic in composition. A transition in ash layer composition is observed at ~160–170 mbsf in which the SiO_2 concentration of the bulk ash layers decreases with depth, while the TiO_2 concentration of the bulk ash layers increases with depth. At ~160–170 mbsf, the ash layers are enriched in elements such as Sc and V, and these elemental changes are indicative of a shift to ash of intermediate to mafic composition at this depth (Fig. 13). Ternary diagrams (Fig. 14) indicate at least two populations of ash spanning a mixing line between relatively more felsic (dacites and rhyolite sources) and more mafic (basalt sources) end members.

Other existing data supports the hypothesis of multiple ash populations. Some of the Site 444 cores possess visually black and chemically basaltic ash, which is a unique aspect for the Shikoku Basin. Refractive indices of volcanic glass and associated minerals have been documented as an effective means for correlating widespread tephra layers (Machida and Arai 1983). Based on the refractive indices of glass shards from ash layers at Site 444, Furuta and Arai (1980) (their Figure 12) show a

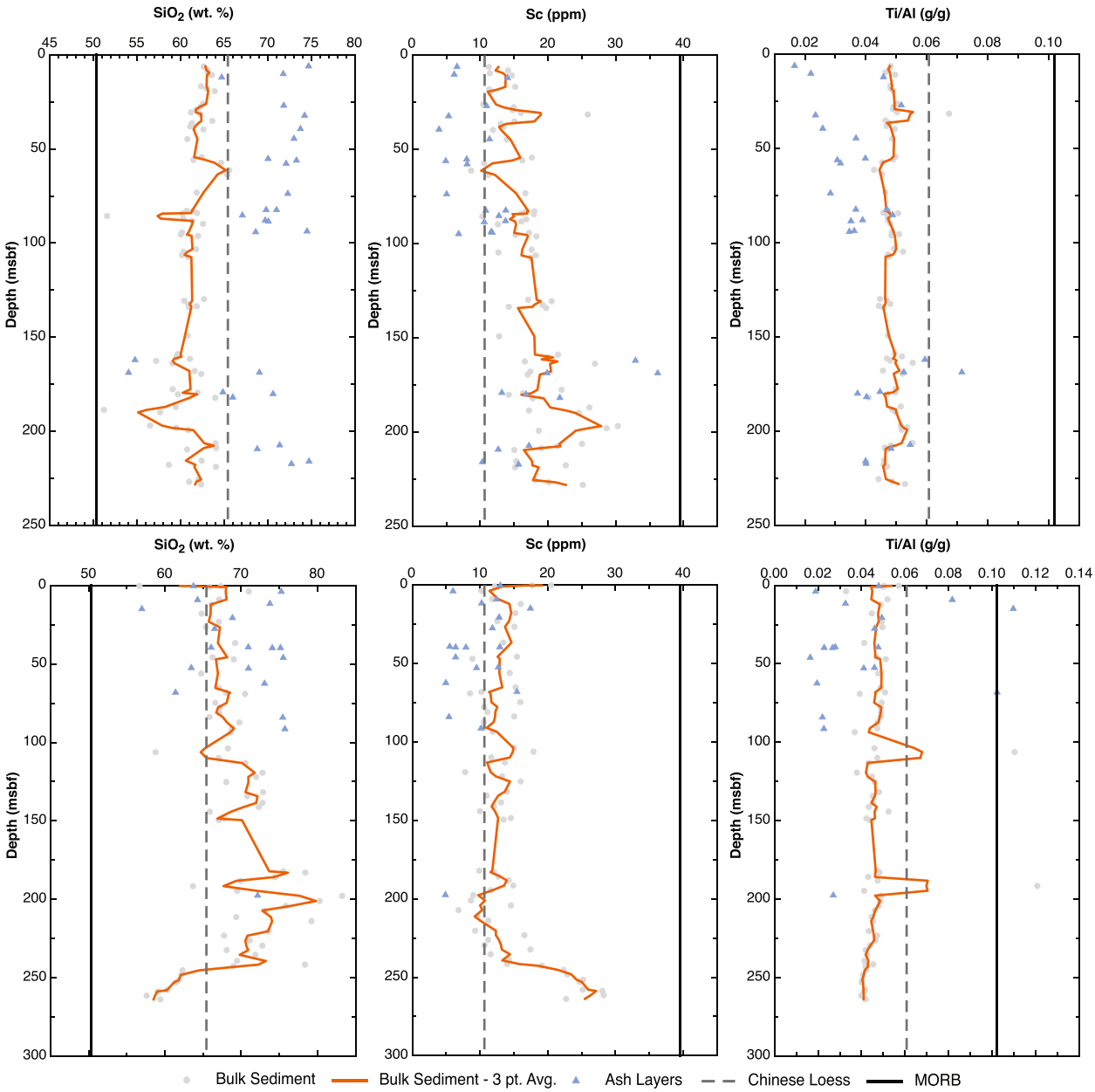

Fig. 13 Representative compositions and elemental ratios plotted with depth. Chinese Loess (Jahn et al. 2001), MORB (Arevalo and McDonough 2010). (*Top*) Site 444. (*Bottom*) Site 579/581

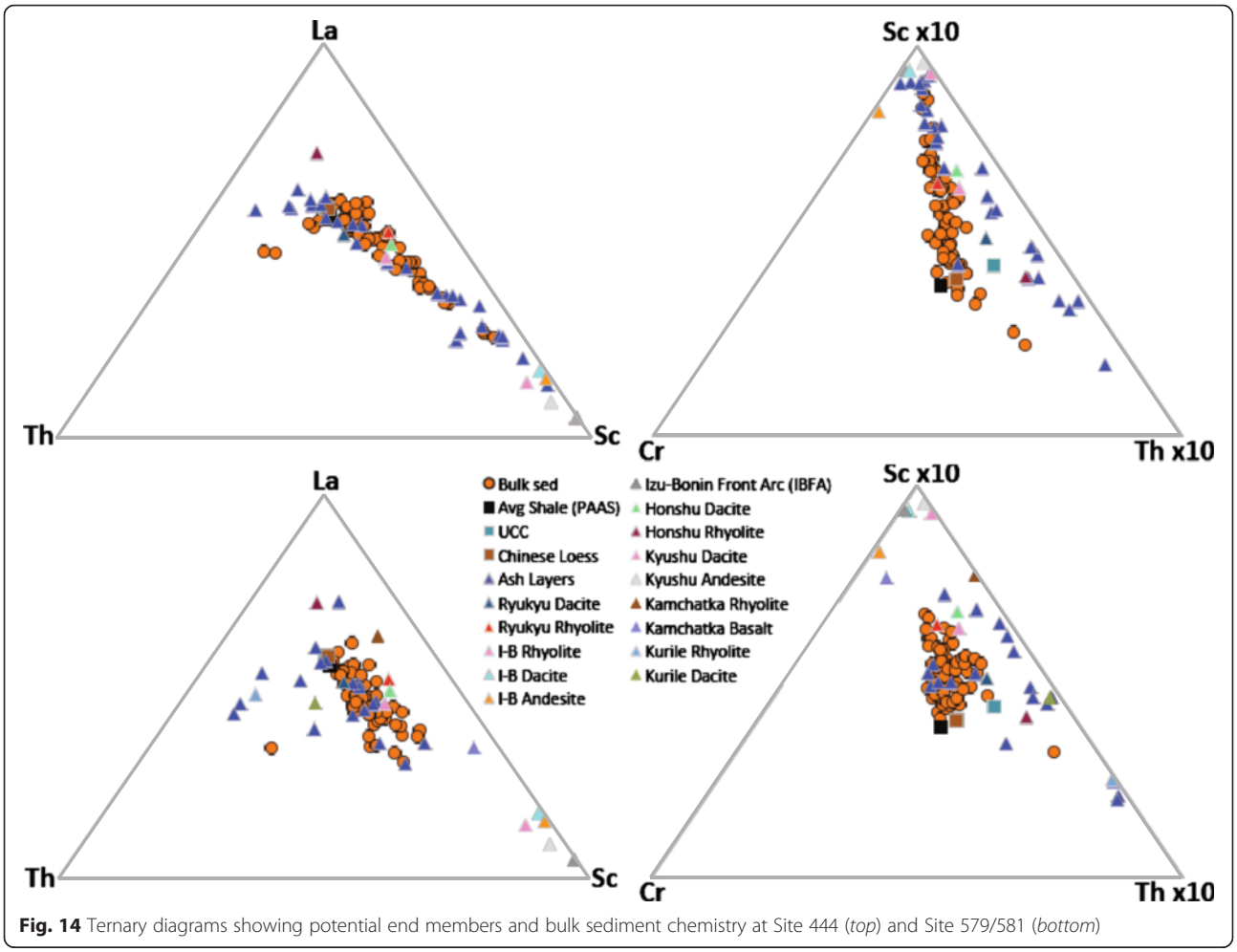

Fig. 14 Ternary diagrams showing potential end members and bulk sediment chemistry at Site 444 (*top*) and Site 579/581 (*bottom*)

linear relationship between refractive index and FeO content. They find that the refractivity of the transition-metal oxides (e.g., FeO, TiO_2, and MnO) at this site is higher than that of SiO_2 and other oxides, thus the refractive index seems to be driven primarily by the transition-metal oxides. The predominate transition-metal oxides in volcanic glass shards are iron-based (i.e., FeO or Fe_2O_3), thus at Site 444 the refractive index of volcanic glass shards can be determined by the content of the iron oxides and indicate that basaltic ashes are present. At Site 444, the ash layers are divided into several groups based on petrographic characteristics, chemical composition, and age. As discussed above, Furuta and Arai (1980) identify rhyolitic and basaltic ash layers at Site 444. Multiple ash populations are also apparent in our microprobe and bulk ash layer chemistry.

Downcore profiles of the bulk sediment do not necessarily provide clear distinction of a single source or two-component mixing (Fig. 13). Additionally, ternary diagrams show that the bulk sediment does not necessarily lie along a mixing line (Fig. 14) with an upper continental component (e.g., Chinese Loess or PAAS) influencing the sediment in addition to the ash components discussed above. Thus, there is likely at least one additional end member beyond the multiple ash populations that influences the bulk sediment composition. This will be explored further in our future studies.

Based on the above discussion of compositional trends, QFA was performed on the data at Site 444 using a modified element suite compared to that used for Site 1149 and Site 52 (Table 1). When performing factor analysis, there is a balance that must be maintained between the number of elements and the number of samples in the dataset. Reimann et al. (2002) outline a number of parameters by which to define the appropriate number of elements. We maintain a very conservative use of these rules, and as such during our study of Site 444, with 71 samples in the dataset, we restricted our element menu to seven (7) elements. Of the refractory elements chosen as representative of the aluminosilicate end members (Al, Ti, Sc, Cr, Ni, Nb, La, Th), Ni overall shows the least variability between potential sources and thus was removed from the element menu for our statistical analysis of Site 444.

Table 1 Bulk sediment elemental composition (ppm) used for QFA analysis, Site 444

Leg	Site	Hole	Core	Type	Section	Top depth (cm)	Bottom depth (cm)	Depth (msbf)	Al (ppm)	Ti (ppm)	Sc (ppm)	Cr (ppm)	Nb (ppm)	La (ppm)	Th (ppm)
58	444	*	2	R	1	24	26	6.24	79,996	3853	11.27	70.41	7.94	29.26	11.58
58	444	*	2	R	2	57	59	8.07	80,559	3832	14.09	68.73	10.92	36.56	10.75
58	444	*	2	R	3	53.5	55.5	9.54	83,039	3853	11.42	77.58	8.36	28.96	12.48
58	444	*	2	R	4	25	27	10.75	84,474	4190	14.67	88.30	12.79	31.16	11.36
58	444	*	3	R	1	124	126	16.74	81,860	3930	15.15	73.85	11.52	32.08	10.63
58	444	*	3	R	2	107.5	109.5	18.08	84,837	4085	11.31	78.40	7.94	30.28	23.13
58	444	*	3	R	3	86	88	19.36	79,428	3889	11.58	63.46	6.84	28.87	13.82
58	444	*	4	R	1	106	108	26.06	82,894	4157	10.43	80.53	6.65	32.58	26.08
58	444	*	4	R	2	108	110	27.58	80,804	3970	14.96	64.32	11.20	29.80	10.11
58	444	*	4	R	3	108	110	29.08	81,114	3965	14.79	66.16	10.00	33.88	9.93
58	444	*	4	R	4	109	111	30.59	78,989	3969	15.99	68.26	11.75	29.27	10.49
58	444	*	4	R	5	46	48	31.46	79,119	5323	25.88	15.44	3.20	10.26	2.67
58	444	*	5	R	1	62	64	35.12	82,536	3834	15.05	66.76	10.52	32.18	11.10
58	444	*	5	R	2	40.5	42.5	36.41	85,835	4087	13.03	81.69	8.47	32.84	11.82
58	444	*	5	R	3	53	55	38.03	76,601	3582	13.45	60.93	11.02	35.68	11.12
58	444	*	5	R	4	64	66	39.64	85,534	4233	11.88	77.77	7.62	32.26	15.33
58	444	*	6	R	1	76	78	44.76	76,374	3713	13.91	67.92	10.15	29.64	10.31
58	444	*	7	R	1	82.5	84.5	54.33	83,010	4126	17.62	68.63	11.54	32.11	10.78
58	444	*	7	R	2	82.5	84.5	55.83	85,068	4160	16.22	66.89	10.94	31.47	10.62
58	444	*	7	R	3	87	89	57.37	78,574	3564	10.59	50.80	5.41	28.56	9.71
58	444	*	7	R	6	86	88	61.31	77,641	3315	8.65	41.39	3.72	24.15	7.96
58	444	*	8	R	1	49	51	63.49	64,239	2914	11.20	21.17	3.33	11.96	4.33
58	444	*	9	R	1	73.5	75.5	73.24	83,958	3897	16.66	44.20	8.50	33.57	10.12
58	444	A	1	R	1	82.5	84.5	82.83	86,300	4026	17.98	65.34	9.35	29.67	10.09
58	444	*	10	R	1	100.5	102.5	83.01	81,435	3842	16.72	72.61	8.44	34.45	8.59
58	444	*	10	R	2	58	60	84.08	85,360	3903	16.11	69.87	11.43	32.10	11.45
58	444	A	1	R	2	86	88	84.36	82,646	4180	17.91	54.83	8.60	26.22	8.16
58	444	A	1	R	3	60	62	85.6	65,077	3067	10.31	47.18	4.61	27.01	7.58
58	444	A	1	R	4	53	55	87.03	84,916	4014	16.79	65.35	10.50	31.42	10.87
58	444	A	1	R	5	77	79	88.27	86,317	4087	16.05	63.91	10.71	30.28	10.35
58	444	A	1	R	6	82	84	89.78	81,209	3897	12.62	57.46	4.99	29.31	8.33
58	444	A	2	R	2	134	136	94.34	80,643	3913	17.20	61.23	8.65	28.27	9.64
58	444	A	2	R	3	96	98	95.46	80,589	4103	15.22	55.74	5.50	28.58	8.52

Table 1 Bulk sediment elemental composition (ppm) used for QFA analysis, Site 444 *(Continued)*

58	444	A	2	R	4	18	20	96.18	78,731	3810	18.30	49.13	8.16	27.02	8.03
58	444	A	3	R	2	74	76	103.24	82,638	4071	17.58	46.40	9.18	25.53	7.54
58	444	A	3	R	3	73	75	104.73	82,775	4320	12.68	55.50	3.79	26.30	7.31
58	444	A	3	R	4	79	81	106.29	85,566	4046	18.19	61.54	8.92	31.96	9.70
58	444	A	3	R	5	53	55	107.53	83,808	3974	17.42	55.99	8.49	30.56	8.95
58	444	A	6	R	1	34	36	129.84	72,532	3238	17.06	57.16	9.60	28.59	9.97
58	444	A	6	R	2	55	57	130.6	84,911	3983	20.53	44.81	7.98	43.70	8.98
58	444	A	6	R	3	94	96	132.49	84,151	4042	19.21	56.38	9.16	29.40	9.67
58	444	A	6	R	4	52	54	133.57	86,082	3811	14.22	65.93	7.13	30.96	11.47
58	444	A	6	R	5	48	50	134.24	87,133	3982	19.72	38.44	7.93	37.25	8.78
58	444	A	8	R	1	74	76	149.24	82,530	3904	12.79	62.99	4.02	27.01	9.03
58	444	A	9	R	1	95.5	97.5	158.96	82,663	4093	21.47	39.19	5.58	18.86	5.19
58	444	A	9	R	2	89	91	160.39	77,146	4000	19.96	47.48	4.25	25.95	6.92
58	444	A	9	R	3	48	50	161.48	76,262	3576	20.69	37.71	5.49	19.33	5.85
58	444	A	9	R	4	65.5	67.5	162.59	74,302	3564	16.57	47.67	4.26	21.70	6.72
58	444	A	9	R	5	37	39	163.8	76,727	4246	26.94	26.36	4.44	16.22	4.59
58	444	A	10	R	1	45	47	167.95	83,868	3826	17.41	49.19	8.77	39.44	9.45
58	444	A	10	R	2	54.5	56.5	169.55	77,551	4036	17.00	28.06	2.93	16.86	4.13
58	444	A	11	R	1	62.5	64.5	177.63	80,760	4019	22.00	43.95	6.23	22.21	5.90
58	444	A	11	R	2	102	104	179.52	77,568	3853	16.32	31.54	3.37	19.58	4.90
58	444	A	11	R	3	30.5	32.5	180.31	73,192	3451	14.22	30.30	2.33	20.26	5.12
58	444	A	11	R	4	68	70	182.18	73,600	3011	17.74	32.50	4.40	18.30	5.17
58	444	A	12	R	1	53.5	55.5	187.04	79,144	4070	26.12	41.96	6.10	19.34	5.91
58	444	A	12	R	2	60	62	188.6	65,137	3165	17.19	39.43	5.67	18.21	5.61
58	444	A	12	R	3	41	43	189.91	76,284	3793	24.56	47.45	6.42	20.07	6.47
58	444	A	13	R	1	95	97	196.95	81,168	4176	30.31	26.61	3.26	12.44	3.16
58	444	A	13	R	2	61	63	198.11	77,704	4165	28.66	39.02	5.47	18.67	5.39
58	444	A	13	R	3	36	38	199.36	76,949	3981	18.65	32.70	8.20	26.95	6.21
58	444	A	14	R	1	83	85	206.33	70,259	3887	25.01	14.61	2.19	9.13	2.06
58	444	A	14	R	2	62	64	207.62	77,583	3748	21.44	30.50	3.88	13.31	3.88
58	444	A	14	R	3	29	31	208.79	73,567	3401	19.02	34.00	4.49	15.12	4.56
58	444	A	14	R	4	22	24	209.64	79,436	3744	15.03	57.19	5.12	22.21	8.21
58	444	A	15	R	1	53	55	215.53	79,550	3659	15.30	31.16	2.72	11.85	4.16

Table 1 Bulk sediment elemental composition (ppm) used for QFA analysis, Site 444 *(Continued)*

58	444	A	15	R	2	125	127	217.75	82,603	3788	22.63	43.75	4.36	17.21	5.07
58	444	A	15	R	3	83	85	218.83	74,140	3484	15.16	37.63	2.89	16.34	4.93
58	444	A	16	R	1	106	108	225.56	79,839	3528	18.10	40.54	8.06	22.48	8.21
58	444	A	16	R	2	79	81	226.79	75,025	3649	20.13	45.88	7.72	20.26	7.33

The results of QFA at Site 444 indicate that three factors (end members) explain 98 % of the variability of the data. This is consistent with the geochemical trends we observe in the bulk data, and the three factors explain 53, 33, and 11 % of the variability of the data respectively (Fig. 15, left). Based on the preliminary modeled compositions of these factors, we interpret that there may be one intermediate crustal source, and at least one dacitic source exhibiting higher Ti/Al ratios, although we cannot differentiate further based on QFA alone. If we were to increase the number of factors, we find that four factors can explain 99 % of the variability of the data, with the four factors explaining 55, 34, 9, and 1 % of the variability of the data, respectively (Fig. 15, right). While this fourth factor is small, we find that it predominantly splits the third factor from the previous QFA and identifies an end member that is dominated by variation in Nb.

In terms of the relative downhole distributions of square factor loadings (Fig. 16), Factor 1 dominates over

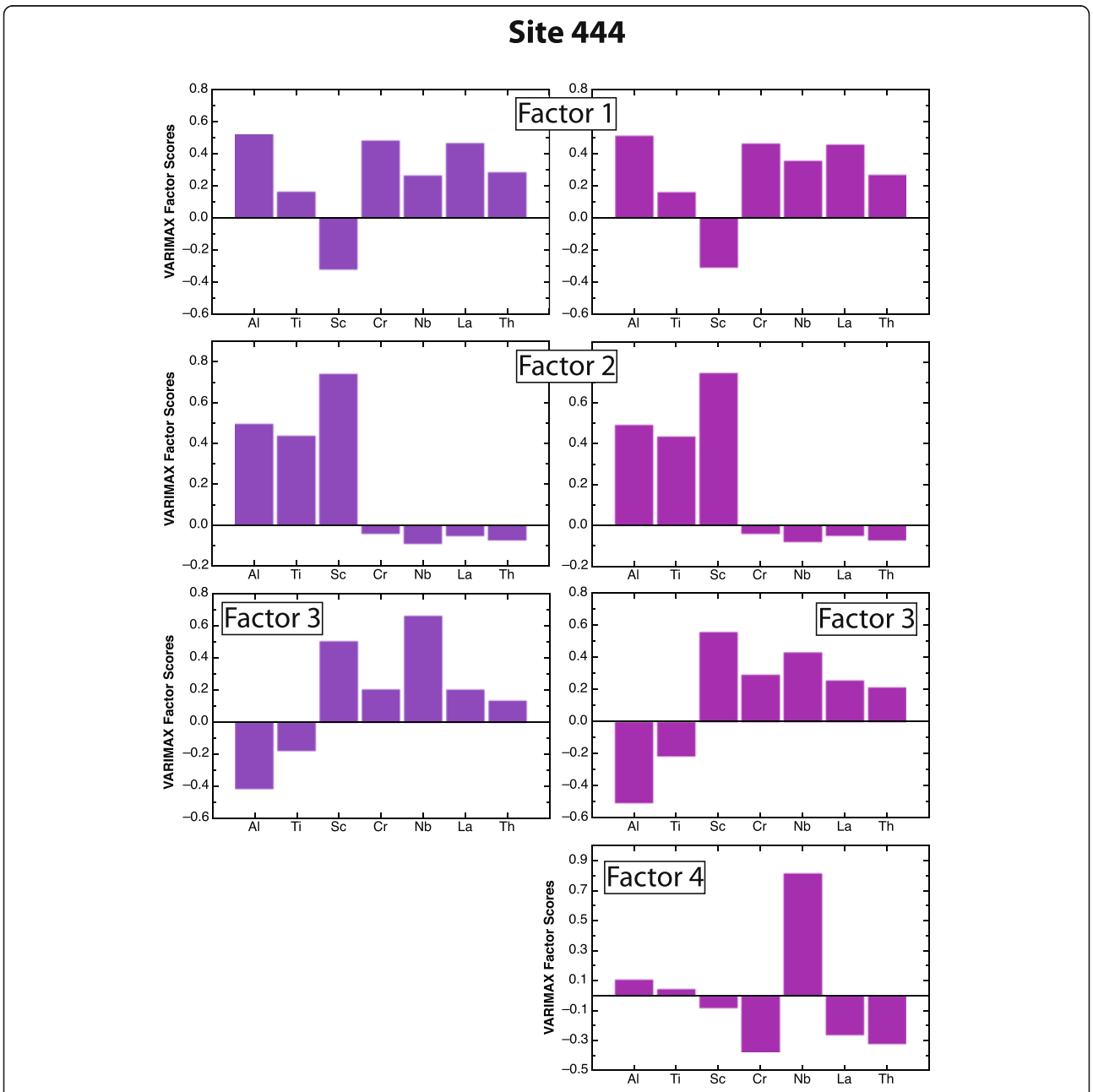

Fig. 15 Site 444, VARIMAX factor scores from QFA. (*Left*) Three-factor model. (*Right*) Four-factor model. As described in the text, Factor 1 is most likely an intermediate crustal source, Factors 2 and/or 3 are most likely dacitic source(s) and Factor 4 is a Nb-rich end member

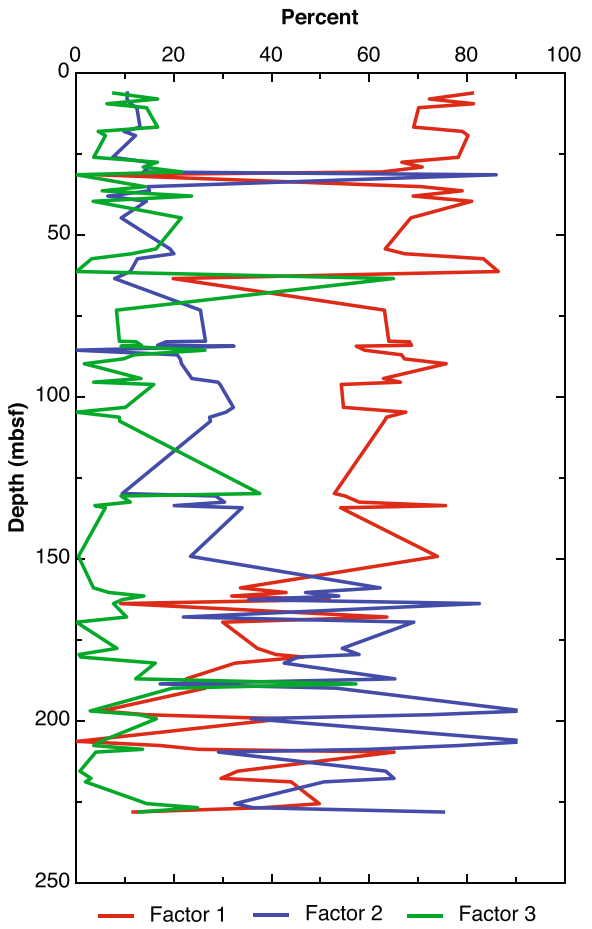

Fig. 16 Depth profiles of square factor loadings from QFA showing the relative contribution of each factor, Site 444

the upper ~150 mbsf and exhibits a broad decrease in importance with depth. Factor 2 is most important in the sequence below ~150 mbsf. Factors 2 and 3 have roughly equal relative contributions over the upper ~50 mbsf, below which Factor 2 exhibits a broad increase while Factor 3 generally decreases. Future statistical analysis by CLS will allow us to determine whether three or four factors are ultimately the appropriate number of end members and will allow us to further determine the sources to the sediment.

Kamchatka and the Kuriles, DSDP Site 579 and Site 581

DSDP Sites 579 and 581 (Fig. 1) were occupied in June 1982 as part of DSDP Leg 86 and were cored as part of a transect across the Kuroshio Current system designed to investigate the paleoceanography of the northwest Pacific. Although spaced relatively far apart, Sites 579 and 581 comprise an excellent composite section of the region (Plank and Langmuir 1998). Site 579 marks the southern margin of the transition between the sediments of the calcareous-siliceous subtropical gyre and the more siliceous subarctic gyre. It was selected for Leg 86 with the goal of compiling a paleoceanographic record of this transition zone for the late Neogene and Quaternary and comparing this record of migrations of the subarctic front with that of Asian eolian inputs. Site 581 is the northernmost of the transect sites drilled during Leg 86 and was designed to provide a high-resolution record of the late Neogene.

As with the other sites in this region, a number of ash layer parameters were examined (Fig. 12). There are no clear trends evident in the number of ash layers through the depth of the site. There are two peaks in the number of ash layers per 5 m, with seven ash layers from 40–45 mbsf and four layers from 80–85 mbsf. This peak at 80 mbsf also corresponds to a peak in total ash thickness (44 cm thick), meaning that not only are more layers present at this depth but also that those layers are thicker. This suggests a period of increased large-scale volcanic eruptions during the Pliocene. However, this is difficult to verify as late Pleistocene glaciations are likely to have obscured the terrestrial record of eruptive history in this area (Volynets et al. 1999). Ash pockets show good correlation with the ash layers in frequency, and we interpret that they originated from disturbance in the core due to the weather during core recovery. The cores had a high occurrence of "flow-in" zones due to heavy seas that may have affected coring and disturbed recovery of some ash layers (Heath et al. 1985).

Interpretation of the bulk ash layers and bulk sediment downhole is not straightforward (Fig. 13). In ternary diagrams, the bulk sediment commonly falls along a mixing line that can be explained by the bulk ash and a relatively more basaltic component, supporting the presence of dispersed ash in the sediment (Fig. 14). Much of the bulk sediment is similar in composition to Chinese Loess, which, while not necessary to explain the composition of the bulk sediment, can be inferred to be almost surely present due to the location of the sites.

Applying QFA to the combined data from these sites, we find that either five or six factors best explain the variability of the data (Table 2, Fig. 17). Comparison of the two sets of factor analysis indicates that Factors 1 through 4 correlate with each other whether there are five or, alternatively, six factors. If there are six factors, Factor 5 from the smaller factor model is split between Factors 5 and 6. Factor 6 explains 1.7 % of the variability of the data in this model, and thus it is interpreted as "real".

Focusing first on the five-factor model, the calculated compositions of the end members identifies Factor 4 (explaining 10.1 % of the variability) as a potential terrigenous source. This is unusual, as in all the other NW pacific sites discussed in this paper the crustal source is the first and/or second end member explaining the

Table 2 Bulk sediment elemental composition (ppm) used for QFA analysis, Sites 579 and 581

Leg	Site	Hole	Core	Type	Section	Top depth (cm)	Bottom depth (cm)	Depth (msbf)	Al (ppm)	Ti (ppm)	Sc (ppm)	Cr (ppm)	Nb (ppm)	La (ppm)	Th (ppm)
86	581	*	1	R	1	28	30	0.28	74,371	4244	20.49	46.23	4.02	16.27	5.36
86	581	*	1	R	1	36	38	0.36	64,845	3268	17.72	39.56	5.38	13.30	4.99
86	579	*	1	H	1	93	95	0.93	70,339	3518	12.17	72.45	6.68	25.01	9.40
86	579	*	1	H	3	75	77	3.75	66,319	2181	10.22	29.39	7.37	8.47	5.93
86	579	*	2	H	1	54	56	8.94	68,056	3532	11.81	58.75	8.02	14.70	6.78
86	579	*	2	H	3	73	75	12.13	73,188	3562	16.02	57.21	8.70	21.20	8.41
86	579	A	1	H	3	94	96	17.94	75,385	3367	15.23	44.72	7.02	15.57	6.65
86	579	A	1	H	7	6	8	23.06	68,144	3364	12.58	54.34	7.94	17.55	6.68
86	579	A	2	H	3	13	15	26.63	69,347	3438	15.07	63.72	9.20	21.34	8.62
86	579	A	3	H	3	73	75	36.73	66,624	2746	13.44	27.85	6.15	10.90	4.88
86	579	A	4	H	3	25	27	45.75	72,574	3398	15.46	59.67	9.37	15.94	7.88
86	579	A	4	H	4	4	6	47.04	43,351	2216	8.89	46.87	8.44	11.55	5.78
86	579	A	5	H	3	107	109	56.07	67,296	3207	14.39	55.31	8.70	21.52	8.26
86	579	A	6	H	3	76	78	65.26	70,026	3410	15.26	57.05	8.74	15.57	7.98
86	579	A	6	H	5	73	75	68.23	53,622	2724	10.20	49.76	6.55	19.78	6.26
86	579	A	6	H	6	10	12	69.1	62,451	2446	8.53	30.52	2.54	17.37	5.54
86	579	A	7	H	3	72	74	74.72	72,871	3585	15.95	59.25	10.44	23.68	9.41
86	579	A	7	H	5	72	74	77.72	68,002	3323	10.60	66.32	4.14	23.43	8.82
86	579	A	8	H	1	52	54	81.02	70,043	3426	11.11	59.48	6.03	23.35	8.69
86	579	A	8	H	3	30	32	83.8	73,144	3565	15.05	61.25	9.79	24.24	9.13
86	579	A	8	H	5	72	74	87.22	59,725	2829	10.54	52.81	6.70	27.02	8.18
86	579	A	9	H	1	110	112	91.1	65,280	3076	10.55	56.03	4.62	21.69	7.78
86	579	A	9	H	3	61	63	93.61	62,214	2294	11.87	38.56	7.77	21.26	8.69
86	579	A	10	H	3	131	133	103.81	64,853	2977	15.04	54.89	7.33	20.29	7.53
86	579	A	10	H	5	72	74	106.22	68,686	7575	17.89	51.60	6.58	15.94	6.28
86	579	A	11	H	1	94	96	109.94	67,054	3167	11.67	57.35	5.18	20.79	8.01
86	579	A	11	H	3	114	116	113.14	60,192	2612	13.67	40.83	6.95	14.15	6.71
86	579	A	12	H	1	83	85	119.33	54,488	2061	7.81	23.08	4.69	19.02	6.70
86	579	A	12	H	3	49	51	121.99	55,246	2474	13.26	41.86	6.21	14.32	6.26
86	579	A	12	H	5	76	78	125.26	63,097	2906	16.01	44.42	5.55	17.65	5.69
86	579	A	13	H	3	74	76	131.74	53,852	2582	13.99	43.75	5.69	12.81	5.30
86	579	A	13	H	5	27	29	134.27	57,088	2580	10.98	50.74	5.24	22.10	6.50
86	579	A	14	H	1	107	109	138.57	54,699	2471	13.11	47.12	6.56	18.01	7.14

Table 2 Bulk sediment elemental composition (ppm) used for QFA analysis, Sites 579 and 581 *(Continued)*

86	579	A	14	H	3	66	68	141.16	55,940	2423	12.06	44.14	6.49	12.61	5.58
86	579	A	14	H	5	70	72	144.2	73,974	3875	10.00	50.23	6.63	19.07	6.45
86	579	A	15	H	2	2	4	148.52	69,270	2925	14.56	55.19	7.95	22.95	8.46
86	579	A	15	H	CC	16	18	149.53	71,892	3146	13.49	62.63	9.86	18.70	9.01
86	581	*	2	R	1	62	64	182.12	42,056	1999	9.89	37.37	2.78	24.82	5.66
86	581	*	2	R	2	2	4	183.02	34,466	1662	12.08	27.39	4.28	18.16	5.07
86	581	*	2	R	3	137	139	185.87	50,664	2181	12.71	28.88	5.89	16.86	5.71
86	581	*	2	R	5	73	75	188.23	61,058	2893	14.22	38.94	5.38	25.91	6.30
86	581	*	3	R	1	58	60	191.58	56,561	6826	14.90	39.01	4.80	14.97	4.67
86	581	*	3	R	3	62	64	194.62	61,976	2550	11.56	33.12	5.22	12.46	4.74
86	581	*	3	R	5	74	76	197.74	27,691	1359	9.00	28.40	4.15	13.98	4.77
86	581	*	4	R	1	57	59	201.07	33,889	1641	8.65	24.95	2.31	15.01	4.71
86	581	*	4	R	3	76	78	204.26	46,571	2231	14.57	47.58	6.51	16.62	7.06
86	581	*	4	R	5	67	69	207.17	30,626	1412	6.83	26.45	1.97	8.75	4.53
86	581	*	5	R	1	126	128	211.26	60,537	2704	9.60	42.27	3.69	12.58	5.50
86	581	*	5	R	3	92	94	213.92	39,316	1781	11.23	32.04	5.22	7.86	4.84
86	581	*	6	R	1	86	88	220.36	51,086	2214	9.28	46.00	2.83	18.85	6.78
86	581	*	6	R	3	67	69	223.17	64,892	3061	16.55	54.76	8.36	18.97	8.96
86	581	*	6	R	5	74	76	226.24	58,477	2715	11.20	50.82	4.27	23.34	9.07
86	581	*	7	R	1	52	54	229.52	54,775	2401	10.65	50.44	3.28	21.27	8.15
86	581	*	7	R	3	36	38	232.36	70,340	2946	17.45	54.41	9.17	16.29	10.10
86	581	*	7	R	5	37	39	235.37	59,378	2529	11.56	50.07	3.26	23.01	8.75
86	581	*	8	R	1	77	79	239.27	63,987	2643	14.31	51.64	5.33	22.36	10.21
86	581	*	8	R	3	11	13	241.61	44,113	2001	14.00	38.89	6.23	17.51	7.56
86	581	*	8	R	3	115	117	242.65	64,594	2703	19.14	47.94	8.11	22.13	10.42
86	581	*	8	R	5	77	79	245.27	83,065	3497	22.35	61.47	10.04	33.19	14.07
86	581	*	9	R	1	16	18	248.16	83,298	3381	22.88	57.87	9.33	31.95	13.20
86	581	*	9	R	3	59	61	251.59	82,323	3316	25.21	57.11	10.80	20.48	13.59
86	581	*	9	R	4	46	48	252.96	85,210	3411	24.70	51.25	9.51	31.48	14.47
86	581	*	10	R	1	42	44	257.92	89,185	3707	25.16	60.99	11.65	34.16	16.84
86	581	*	10	R	1	124	126	258.74	86,271	3549	28.05	55.41	11.20	39.01	17.72
86	581	*	10	R	3	92	94	261.42	88,986	3546	28.26	55.69	11.63	17.12	11.30

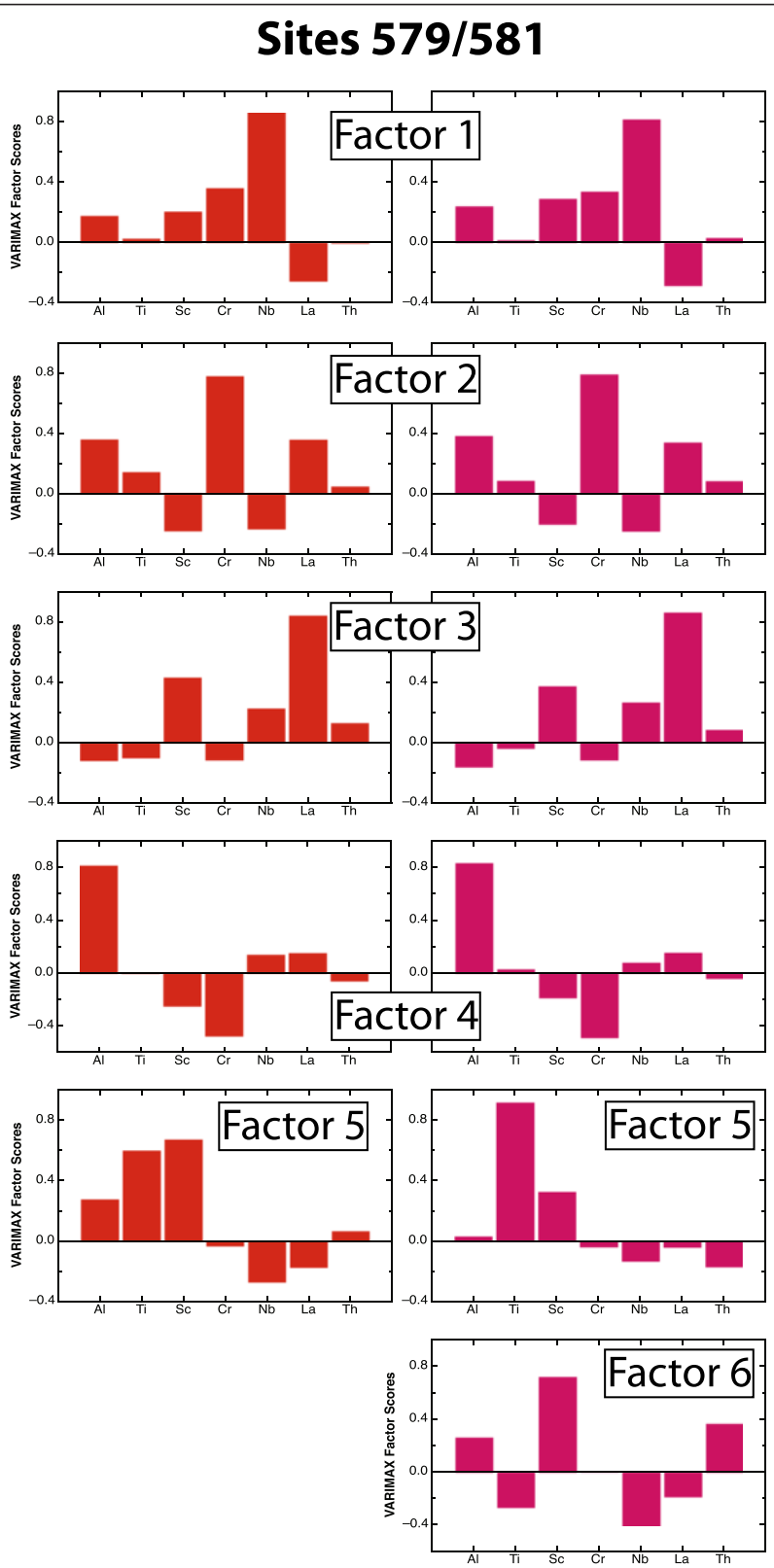

Fig. 17 Sites 579 and 581, VARIMAX factor scores from QFA

majority of the variability in the dataset. This speaks to the importance of dispersed ash at Site 579/581, since the dispersed ash component(s) appear to be controlling most of the variability. This will be further explored in future work. The six-factor model identifies a few factors that are dominated by a single element (Al in Factor 4, Ti in Factor 5) indicating that the division of factors is controlling variability as opposed to their specific concentrations.

As with Site 444, square factor loadings for these Kamchatka/Kurile sites can allow us to assess the relative contribution of the individual factors on a sample-by-sample basis (Fig. 18). In order to assess the relative contributions for this work, we will focus here on the five-factor model. We observe that for most of the sedimentary record, Factor 1 dominates the record, although from ~65 to ~93 mbsf, Factor 2 is the dominate component. Additionally, from ~150 to ~240 mbsf the variance in the record is dominated by Factor 3 (~150 to ~200 mbsf) or Factor 2 (~200 to ~240 mbsf). Factors 4 and 5 are remarkably similar in importance until ~200 mbsf below which Factor 4 increases in relative importance while Factor 5 remains fairly stable. Future statistical analysis by CLS will allow us to determine whether five or six factors are ultimately the appropriate number of end members and will allow us to further determine the sources to the sediment.

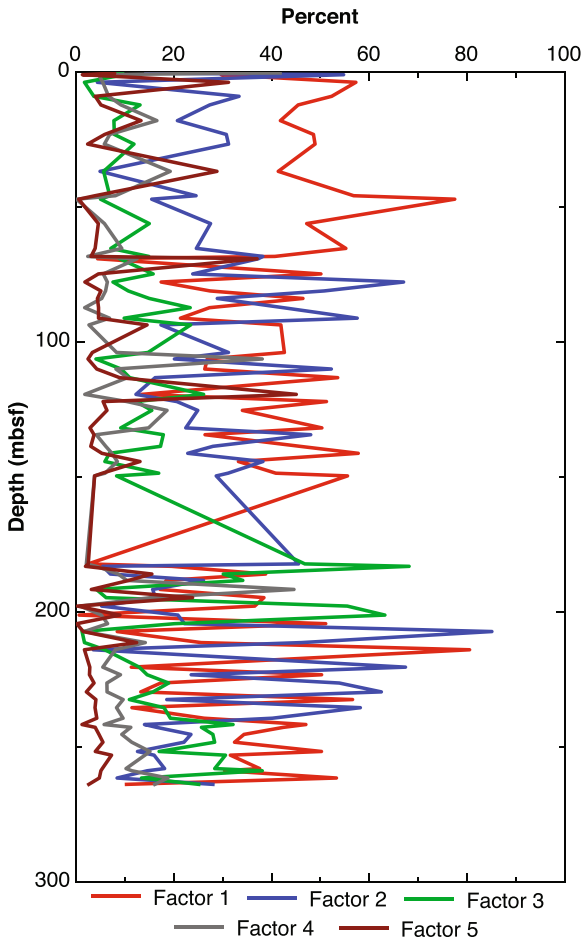

Fig. 18 Depth profiles of square factor loadings from QFA showing the relative contribution of each factor, Sites 579 and 581

Conclusions

Although the presence of dispersed ash in marine sediment has been long known by marine sedimentologists, the overall quantification of its abundance and its composition has recently received renewed attention. The dispersed ash, either altered or unaltered, is extremely difficult to differentiate from detrital/terrigenous/authigenic clay as they are all, fundamentally speaking, "aluminosilicates". The combined geochemical (major, trace, REEs) and statistical (Pisias et al. 2013) approach provides the chemical context for the determination of provenance and the distinctive resolution of the different aluminosilicate components based on their individual geochemical signature(s).

The case studies we present here show that this approach can be useful in multiple different arc systems. We have also shown that by adding the dispersed ash component to the study of discrete ash layers, many additional geological and oceanographic interpretations can be uncovered. Most obviously, we have shown how geochemical modeling of the bulk sediment composition can indicate the presence of an additional ash source that is not recorded in the discrete layer record. Furthermore, in cores where there are no remaining discrete layers (either due to natural bioturbation or man-made coring disturbance), we show that important ash contributions may still be recognized and studied for their composition and accumulation. We have also shown how the accumulation of dispersed ash will either best correlate with the *thickest* ash layer, or alternatively, the *frequency* of the discrete ash layers, which lead to dramatically different interpretations regarding the volcanic mechanisms of a given arc. Finally, when considering these studies throughout the northwest Pacific Ocean, or in marginal basins such as the Japan Sea, our approach may be used to develop a mass balance inventory of the total mass of volcanic ash that is more accurate than estimates based solely on the combined thicknesses of the discrete layers.

There are many other future research directions that are a natural extension of the work described above. There are a number of regions for which the characterization of the abundance and extent of dispersed ash would be of great scientific and societal importance (e.g., Tonga, Costa Rica, and Indonesia), and studying the dispersed ash component in these regions will most certainly lead to an improved understanding of explosive volcanism in those

systems. Moreover, most marine volcanoes are beneath the sea surface, either in mid-ocean ridge settings or in convergent margins (e.g., Fiske et al. 2001; White et al. 2003). The vast majority of these eruptions go unobserved and their products are often unrecovered and thus are understudied. Often the only evidence of subaqueous eruptions are widespread pumice rafts. Little is known, however, about the fate of these rafts, yet they too are likely to contribute dispersed ash to the sediment.

Volcanic ash may have significant nutrient fertilization potential as well. Particulate matter from large volcanic eruptions may release enough iron and other nutrients to the surface ocean to stimulate primary production over short time scales (Watson 1997; Olgun et al. 2011). Thus, it would be important to develop an understanding of the effects of iron and other elements from volcanic ash on the biological productivity of the open ocean and, second, to consider the biological effects of volcanic ash-driven elemental fertilization in the open ocean through Earth's history. The use of the dispersed ash record can be applied to achieve these goals.

Additionally, ash, with its major component being volcanic glass, is a metastable phase with high potential biological availability to the subseafloor ecosystem, may provide both electron donors and electron acceptors important to microbial energetics. Characterizing the chemistry of the subseafloor sediment will provide vital information about the nutrients available to subseafloor microbial life as well as the pathways by which these nutrients are utilized.

Abbreviations

BNN: Izu-Bonin Boninite; CL: Chinese Loess; CLS: Constrained Least Squares; CRISP II: Costa Rica Seismogenesis Project Stage II; DSDP: Deep Sea Drilling Project; HR: Honshu Rhyolite; IBA: Izu-Bonin Andesite; IBFA: Izu-Bonin Front Arc; IBR: Izu-Bonin Rhyolite; ICP-ES: Inductively Coupled Plasma-Emission Spectrometer; ICP-MS: Inductively Coupled Plasma-Mass Spectrometer; IODP: Integrated Ocean Drilling Program; LRC: lower red clay MAR, mass accumulation rate; MORB: Mid-Ocean Ridge Basalt; ODP: Ocean Drilling Program; PAAS: Post-Archean average Australian Shale; PGL: pale green laminae; QFA: Q-Mode Factor Analysis; RCB: Rotary Core Barrel; REE: rare earth element; TI: Total Inversion; URC: upper red clay.

Competing interests

The authors' declare that they have no competing interests.

Authors' contributions

RPS is the lead author of the paper, performed the ICP-ES and ICP-MS analyses, and led the research and multiple conversations/interactions with the research team. RWM funded the research (see Acknowledgements), performed the oversight of the project, advised then-Ph.D. student RPS and then-undergraduate students SG, RL, and CCM, facilitated the discussion with co-authors and community, and contributed the text. JCS and SK performed microprobe analyses of volcanic glass from ash layers, discussed the research, contributed revisions of the text, compiled the reference list, created Figs. 1, 2, and 4, and provided the interpretation of the data. SK funded the research (see Acknowledgements) and advised Ph.D. student JCS regarding ash chemistry. FH reviewed and revised the manuscript. MBU discussed the research, contributed the revisions of the text, and provided the interpretation of the data. SG, RL, and CCM assisted in the ICP-ES and ICP-MS analyses, were involved in the preliminary statistics and interpretations of Sites 52, 444, and 579/581, and reviewed and commented on the manuscript. All authors read and approved the final manuscript.

Acknowledgements

This research used samples and/or data provided by the IODP. RPS and RWM thank the US Science Support Program (USSSP) of IODP, NSF OCE-0136855, and NSF OCE-0958002 for financial support, and T. Ireland, A. G. Dunlea, N. Murphy, and J. W. Sparks for laboratory assistance. JCS and SK thank the German Research Foundation for financial support (KU-2685/1-1, 2-1&2) and M. Thöner, K. Strehlow for laboratory assistance. Portions of this material are based upon work supported while RWM was serving at the National Science Foundation. Thanks to those who reviewed and commented on the manuscript.

Author details

[1]Department of Earth & Environment, Boston University, Boston, MA 02215, USA. [2]GEOMAR Helmholtz Centre for Ocean Research Kiel, 24148 Kiel, Germany. [3]Department of Earth and Environmental Science, New Mexico Institute of Mining and Technology, Socorro, NM 87801, USA. [4]Department of Geosciences, Princeton University, Princeton, NJ 08544, USA. [5]Division of Earth and Ocean Sciences, Nicholas School of the Environment, Duke University, Durham, NC 27708, USA. [6]Department of Oceanography, Texas A&M University, College Station, TX 77843, USA.

Received: 30 April 2015 Accepted: 21 December 2015
Published online: 04 January 2016

References

Arevalo R, McDonough WF. Chemical variations and regional diversity observed in MORB. Chem Geol. 2010;271(1):70–85.

Bailey JC. Geochemical history of sediments in the northwestern Pacific Ocean. Geochem J. 1993;27:71–90.

Bailey JC. Role of subducted sediments in the genesis of Kurile-Kamchatka island arc basalts: Sr isotopic and elemental evidence. Geochem J. 1996; 30(5):289–321.

Bryan SE, Cook A, Evans JP, Colls PW, Wells MG, Lawrence MG, et al. Pumice rafting and faunal dispersion during 2001-2002 in the Southwest Pacific: record of a dacitic submarine explosive eruption from Tonga. Earth Planet Sci Lett. 2004;227(1-2):135–54.

Bryant CJ, Arculus RJ, Eggins SM. Laser ablation-inductively coupled plasmamass spectrometry and tephras: a new approach to understanding arc-magma genesis. Geology. 1999;27(12):1119–22.

Bryant CJ, Arculus RJ, Eggins SM. The geochemical evolution of the Izu–Bonin arc system: a perspective from tephras recovered by deep-sea drilling. Geochem Geophys Geosyst. 2003;4(11):1094. doi:10.1029/2002GC000427.

Bursik M. Effect of wind on the rise height of volcanic plumes. Geophys Rese Lett. 2001;28(18):3621–4.

Cambray H, Cadet JP, Pouclet A. Ash layers in deep-sea sediments as tracers of arc volcanic activity: Japan and Central America as case studies. Island Arc. 1993;2:72–86.

Cambray H, Pubellier M, Jolivet L, Pouclet A. Volcanic Activity Recorded in Deep-Sea Sediments and the Geodynamic Evolution of Western Pacific Island Arcs, in Active Margins and Marginal Basins of the Western Pacific (eds B. Taylor and J. Natland), American Geophysical Union, Washington, DC; 1995. doi:10.1029/GM088p0097.

Carey SN. Influence of convective sedimentation on the formation of widespread tephra fall layers in the deep sea. Geology. 1997;25(9):839–42.

Carey SN, Sigurdsson H. Deep-sea evidence for distribution of tephra from the mixed magma eruption of the Soufriére on St Vincent 1902: ash turbidites and airfall. Geology. 1978;6:271–4.

Carey SN, Sigurdsson H. The Roseau ash: Deep-sea tephra deposits from a major eruption on Dominica, Lesser Antilles arc. J Volcanol Geoth Res. 1980;7:67–86.

Carey SN, Sigurdsson H. Grain size of Miocene volcanic ash layers from Sites 998 999 and 1000: Implications for source areas and dispersal. Proc Ocean Drill Program Sci Results. 2000;165:101–10.

Carey SN, Sparks RSJ. Quantitative models of fallout and dispersal of tephra from volcanic eruption columns. Bull Volcanol. 1986;48:109–25.

Carey RJ, Houghton BF, Thordarson T. Tephra dispersal and eruption dynamics of wet and dry phases of the 1875 eruption of Askja Volcano Iceland. Bull. 2010;72(3):259–78.

Chan LH, Kastner M. Lithium isotopic compositions of pore fluids and sediments in the Costa Rica subduction zone: implications for fluid processes and sediment contribution to the arc volcanoes. Earth Planet Sci Lett. 2000;183(1):275–90.

deVries Klein G, Kobayashi K. Initial Reports of the Deep Sea Drilling Project v. 58. Washington DC: US Government Printing Office; 1980. p. 1022.
deVries Klein G, McConville RL, Harris JM, Steffensen CK. Petrology and Diagenesis of Sandstones Deep Sea Drilling Project Site 445 Daito Ridge. Init Rep DSDP. 1980;58:609–16. doi:10.2973/dsdpproc581121980.
Duggen S, Olgun N, Croot P, Hoffmann LJ, Dietze H, Delmelle P, et al. The role of airborne volcanic ash for the surface ocean biogeo- chemical iron-cycle: A review. Biogeosci. 2010;7:827–44. doi:10.5194/bg-7-827-2010.
Dunlea AG, Murray RW, Sauvage J., Pockalny RA, Spivack AJ, Harris RN, et al. Cobalt-based age models of pelagic clay in the South Pacific Gyre. Geochem Geophys Geosys. 2015a;16. doi:10.1002/2015GC005892.
Dunlea AG, Murray RW, Sauvage J, Pockalny RA, Spivack AJ, Harris RN, et al. Dust, volcanic ash, and the evolution of the South Pacific Gyre through the Cenozoic. Paleocean. 2015b; 30. doi:10.1002/2015PA00282.
Dymond J. Geochemistry of Nazca plate surface sediments: an evaluation of hydrothermal biogenic detrital and hydrogenous sources. Geol Soc Am Memoirs. 1981;154:133–74.
Expedition 340 Scientists Lesser Antilles volcanism and landslides: Implications for hazard assessment and long-term magmatic evolution of the arc. Prelim Rep Integrated Ocean Drill Program 340. 2012. doi:10.2204/iodppr3402012.
Fischer AG, Heezen BC, Boyce RE, Bukry D, Douglas RG, Garrison RE, et al. Site 52. Initial Rep Deep Sea Drill Proj 6:247–290. 1971. doi:10.2973/dsdpproc61101971.
Fisher RV, Schmincke H-U. Pyroclastic rocks. New York: Springer-Verlag; 1984. p. 472.
Fiske RS, Naka J, Iizasa K, Yuasa M, Klaus A. Submarine silicic caldera at the front of the Izu-Bonin arc Japan: voluminous seafloor eruptions of rhyolite pumice. Geol Soc Amer Bull. 2001;113:813–24.
Freundt A, Grevemeyer I, Rabbel W, Hansteen TH, Hensen C, Wehrmann H, et al. Volatile (H_2O, CO_2, Cl, S) budget of the Central American subduction zone. Int J Earth Sci. 2014;103(7):2101–27. doi:10.1007/s00531-014-1001-1.
Frogner P, Gíslason SR, Óskarsson N. Fertilizing potential of volcanic ash in ocean surface water. Geology. 2001;29:487–90.
Furuta T, Arai F. Petrographic and geochemical properties of tephras in Deep Sea Drilling Project cores from the north Philippine Sea. Init Rep DSDP. 1980;58: 617–27. doi:10.2973/dsdpproc581131980.
Gardner JV, Nelson CS, Baker PA. Distribution and character of pale-green laminae in sediment from Lord Howe Rise: A probable late Neogene and Quaternary tephrostratigraphic record. In Blakeslee JH (ed) Initial Reports of the DSDP 90, Wahsington, 1986. p. 1145–1158.
Hauff F, Hoernle K, Schmidt A. Sr-Nd-Pb composition of Mesozoic Pacific oceanic crust (Site 1149 and 801 ODP Leg 185): Implications for alteration of ocean crust and the input into the Izu-Bonin-Mariana subduction system. Geochem Geophys Geosyst. 2003;4(8):8913. doi:10.1029/2002GC000421.
Heath GR, Kovar RB, Lopez C, Campi GL. Elemental composition of Cenozoic pelagic clays from deep sea drilling project sites 576 and 578 Western North Pacific. Init Rep DSDP. 1985;86:605–48. doi:10.2973/dsdpproc861271985.
Hein JR, Scholl DW, Barron JA, Jones MG, Miller J. Diagenesis of late Cenozoic diatomaceous deposits and formation of the bottom simulating reflector in the southern Bering Sea. Sedimentol. 1978;25(2):155–81.
Henry P, Kanamatsu T, Moe K, Expedition 333 Scientists. Proceedings IODP 333, Tokyo Integrated Ocean Drilling Program Management, International Inc Washington DC; 2012. doi:10.2204/iodpproc3332012.
Hochstaedter A, Gill J, Peters R, Broughton P, Holden P, Taylor B. Across-arc geochemical trends in the Izu-Bonin arc: Contributions from the subducting slab Geochem Geophys Geosys. 2001;2(7). doi:10.1029/2000GC000105.
Hovan SA, Rea DK, Pisias NG. Late Pleistocene continental climate and oceanic variability recorded in northwest Pacific sediments. Paleoceanography. 1991;6(3):349–70.
Huang TC. A volcanic sedimentation model: Implications of processes and responses of deep-sea ashes. Mar Geol. 1980;38:103–22.
Huang TC, Watkins ND, Shaw DM, Kennett JP. Atmospherically transported volcanic dust in South Pacific deep sea sedimentary cores at distances over 3000 km from the eruptive source. Earth Planet Sci Lett. 1973;20(1):119–24.
Huang TC, Fillon RH, Watkins ND, Shaw DM. Volcanism and silicious microfaunal diversity in the southwest Pacific during the Pleistocene period. Deep-Sea Res. 1974;21:377–84.
Huang TC, Watkins ND, Shaw DM. Atmospherically transported volcanic glass in deep-sea sediments: volcanism in sub-antarctic latitudes of the south Pacific during late Pliocene and pleistocene time. Bull Geol Soc Am. 1975;86(9):1305–15.
Hüpers A, Ikari MJ, Dugan B, Underwood MB, Kopf AJ. Origin of a zone of anomalously high porosity in the subduction inputs to Nankai Trough. Mar Geol. 2015;361:47–162.
Hyeong K, Park S, Yoo CM, Kim K. Mineralogical and geochemical compositions of the eolian dust from the northeast equatorial Pacific and their implications on paleolocation of the Intertropical Convergence Zone. Paleoceanography. 2005;20(0883-8305). doi:10.1029/2004PA001053.
Jahn BM, Gallet S, Han JM. Geochemistry of the Xining Xifeng and Jixian sections Loess Plateau of China: eolian dust provenance and paleosol evolution during the last 140 ka. Chem Geol. 2001;178(1–4):71–94.
Jones MT, Gíslason SR. Rapid releases of metal salts and nutrients following the deposition of volcanic ash into aqueous environments. Geochim Cosmochim Acta. 2008;72:3661–80. doi:10.1016/jgca200805030.
Jordan BR, Sigudsson H, Carey SN, Rogers R, Ehrenborg J. Geochemical correlation of Caribbean Sea tephra layers with ignimbrites in Central AmericaGeological Society of America Special Papers. 2006; 402:175–208. doi:10.1130/2006.2402(08).
Kastner M, Elderfield H, Martin JB. Fluids in convergent margins: what do we know about their composition origin role in diagenesis and importance for oceanic chemical fluxes? Philos Trans R Soc Lond A. 1991;335(1638):243–59.
Kennett JP, McBirney AR, Thunell RC. Episodes of Cenozoic volcanism in the circum-Pacific region. J Volc Geo Res. 1977;2:145–63.
Klinkhammer GP, Elderfield H, Edmond JM, Mitra A. Geochemical implications of rare earth element patterns in hydrothermal fluids from mid-ocean ridges. Geochim Cosmochim Acta. 1994;58(23):5105–13.
Kryc KA, Murray RW, Murray DW. Al-to-oxide and Ti-to-organic linkages in biogenic sediment: relationships to paleo-export production and bulk Al/Ti. Earth Planet Sci Lett. 2003;211(1):125–41.
Kutterolf S, Freundt A, Peréz W, Mörz T, Schacht U, Wehrmann H, et al. The Pacific offshore record of Plinian arc volcanism in Central America part 1: Along-arc correlations. Geochem Geophys Geosyst. 2008a;9(2). doi:10.1029/2007GC001631.
Kutterolf S, Freundt A, Peréz W. The Pacific offshore record of Plinian arc volcanism in Central America part 2: Tephra volumes and erupted masses. Geochem Geophys Geosys. 2008b;9(2). doi:10.1029/2007GC001791.
Kutterolf S, Freundt A, Schacht U, Bürk D, Harders R, Mörz T, et al. The Pacific offshore record of Plinian arc volcanism in Central America part 3: Application to forearc geology. Geochem Geophys Geosys. 2008c;9(2). doi:10.1029/2007GC001826.
Kutterolf S, Jegen M, Mitrovica JX, Kwasnitschka T, Freundt A, Huybers P. A detection of Milankovitch frequencies in global volcanic activity. Geology. 2013;41(2):227–30. doi:10.1130/G334191.
Kutterolf S, Schindlbeck JC, Scudder RP, Murray RW, Pickering KT, Freundt A, et al. Large volume submarine ignimbrites in the Shikoku Basin: an example for explosive volcanism in the Western Pacific during the Late Miocene. Geochem Geophys Geosys. 2014;15(5):1837–51.
Kyte FT, Leinen M, Heath GR, Zhou L. Cenozoic sedimentation history of the central North Pacific: inferences from the elemental geochemistry of core LL44-GPC3. Geochim Cosmochim Acta. 1993;57:1719–49.
Le Friant A, Ishizuka O, Stroncik NA and the Expedition 340 Scientists (2013) Proceedings of Integrated Ocean Drilling Program vol 340, Tokyo. doi:10. 2204/iodp.proc.340.104.2013
Ledbetter MT, Sparks RSJ. Duration of large-magnitude explosive eruptions deduced from graded bedding in deep-sea ash layers. Geology. 1979;7:240–4.
Lee J, Stern RJ, Bloomer SH. Forty million years of magmatic evolution in the Mariana arc: the tephra glass record. J Geophys Res. 1995;100(B9):17671–87.
Leinen M. The origin of paleochemical signatures in North Pacific pelagic clays: partitioning experiments. Geochim Cosmochim Acta. 1987;51(2):305–19.
Leinen M, Pisias N. An objective technique for determining end-member compositions and for partitioning sediments according to their sources. Geochim Cosmochim Acta. 1984;48(1):47–62.
Lowe DJ. Tephrochronology and its application: a review. Quat Geochronol. 2011; 6:107–53. doi:10.1016/j.quageo.2010.08.003.
Machida H, Arai F. Extensive ash falls in and around the Sea of Japan from large late Quaternary eruptions. J Volc Geotherm Res. 1983;18(1):151–64.
Mackenzie FT, Garrels RM. Chemical mass balance between rivers and oceans. Am J Sci. 1966;264(7):507–25.
Mahony SH, Wallace LM, Miyoshi M, Villamor P, Sparks RSJ, Hasenaka T. Volcano-tectonic interactions during rapid plate-boundary evolution in the Kyushu region SW Japan. Geol Soc Am Bull. 2011;123:2201–23.
Maicher D, White JDL. The formation of deep-sea Limu o Pele. Bull Volcanol. 2001;63:482–96.
Martinez NC, Murray RW, Thunell RC, Peterson LC, Muller-Karger F, Astor Y, et al. Modern climate forcing of terrigenous deposition in the tropics (Cariaco Basin Venezuela). Earth Planet Sci Lett. 2007;264(3):438–51.

Martinez NC, Murray RW, Dickens GR, Kölling M. Discrimination of sources of terrigenous sediment deposited in the central Arctic Ocean through the Cenozoic. Paleoceanography. 2009;24(1). doi:10.1029/2007PA001567.
Martinez NC, Murray RW, Thunell RC, Peterson LC, Muller-Karger F, Lorenzoni L, et al. Local and regional geochemical signatures of surface sediments from the Cariaco Basin and Orinoco Delta Venezuela. Geology. 2010;38(2):159–62.
Metzner D, Kutterolf S, Toohey M, Timmreck C, Niemeier U, Freundt A, et al. Radiative forcing and climate impact resulting from SO2 injections based on a 200,000 year record of Plinian eruptions along the Central American Volcanic Arc. Int J Earth Sci. 2014;103(7):2063–79. doi:10.1007/s00531-012-0814-z.
Murray RW, Leinen M. Chemical transport to the seafloor of the equatorial Pacific Ocean across a latitudinal transect at 135 W: tracking sedimentary major trace and rare earth element fluxes at the Equator and the Intertropical Convergence Zone. Geochim Cosmochim Acta. 1993;57(17):4141–63.
Murray RW, Leinen M. Scavenged excess aluminum and its relationship to bulk titanium in biogenic sediment from the central equatorial Pacific Ocean. Geochim Cosmochim Acta. 1996;60(20):3869–78.
Murray RW, Leinen M, Isern A. Biogenic flux of Al to sediment in the central equatorial Pacific Ocean: evidence for increased productivity during glacial periods. Paleoceanography. 1993;8(5):651–70.
Murray RW, Leinen M, Murray DW, Mix AC, Knowlton CW. Terrigenous Fe input and biogenic sedimentation in the glacial and interglacial equatorial Pacific Ocean. Global Biogeochem Cycles. 1995;9(4):667–84.
Murray RW, Knowlton C, Leinen M, Mix AC, Polsky CH. Export production and carbonate dissolution in the central equatorial Pacific Ocean over the past 1 Myr. Paleoceanography. 2000;15(6):570–92.
Ninkovich D, Sparks RSJ, Ledbetter MT. The exceptional magnitude and intensity of the Toba eruption Sumatra: an example of the use of deep-sea tephra layers as a geological tool. Bull Volcanol. 1978;41:286–98.
Olgun N, Duggen S, Croot PL, Delmelle P, Dietze H, Schacht U, et al. Surface ocean iron fertilization: the role of subduction zone and hotspot volcanic ash and fluxes into the Pacific Ocean Global Biogeochemical Cycles. 2011;25. doi:10.1029/2009GB003761
Peacock SA. Fluid processes in subduction zones. Science. 1990;248(4953):329–37.
Peters JL, Murray RW, Sparks J, Coleman DS. Terrigenous matter and dispersed ash in sediment from the CaribbeanSea: results from Leg 165. Proc Ocean Drill Program Sci Results. 2000;165:115–24. doi:10.2973/odpprocsr1650032000.
Pickering KT, Underwood MB, Saito S, Naruse H, Kutterolf S, Scudder RP, et al. Depositional architecture provenance and tectonic/eustatic modulation of Miocene submarine fans in the Shikoku Basin: results from Nankai Seismogenic Zone experiment. Geochem Geophys Geosys. 2013;14:6. doi:10.1002/ggge.20107.
Piepgras DJ, Jacobsen SB. The behavior of rare earth elements in seawater: precise determination of variations in the North Pacific water column. Geochim Cosmochim Acta. 1992;56(5):1851–62.
Pisias NG, Murray RW, Scudder RP. Multivariate statistical analysis and partitioning of sedimentary geochemical data sets: General principles and specific MATLAB scripts. Geochem Geophys Geosys. 2013;14(10):4015–20. doi:10.1002/ggge20247.
Plank T. Constraints from Thorium/Lanthanum on sediment recycling at subduction zones and the evolution of continents. J Petrol. 2005;46:921–44.
Plank T, Langmuir CH. The chemical composition of subducting sediment and its consequences for the crust and mantle. Chem Geol. 1998;145(3–4):325–94.
Plank T, Ludden JN, Escutia C, et al. Proc Ocean Drill Program Init Results. 2000; 185:1–190. doi:10.2973/odpprocir1852000.
Plank T, Kelley KA, Murray RW, Stern LQ. Chemical composition of sediments subducting at the Izu–Bonin trench. Geochem Geophys Geosyst. 2007;8: Q04I16. doi:10.1029/2006GC001444.
Presti M, Michalopoulos P. Estimating the contribution of the authigenic mineral component to the long-term reactive silica accumulation on the western shelf of the Mississippi River Delta. Cont Shelf Res. 2008;28(6):823–38.
Rea DK. The palcoclimatic record provided by eolian deposition in the deep sea: the geologic history of wind. Rev Geophys. 1994;32:159–95.
Rea DK, Leinen M. Asian aridity and the zonal westerlies: Late Pleistocene and Holocene record of eolian deposition in the northwest Pacific Ocean. Palaeogeog Palaeoclimatol Palaeoecol. 1988;66(1-2):1–8.
Rea DK, Snoeckx H, Joseph LH. Late Cenozoic eolian deposition in the North Pacific: Asian drying Tibetan uplift and cooling of the northern hemisphere. Paleoceanography. 1998;13(3):215–24.
Reid P, Carey SN, Ross DR. Late quaternary sedimentation in the Lesser Antilles island arc. Geol Soc Am Bull. 1996;108:78–100.
Reimann C, Filzmoser P, Garrett RG. Factor analysis applied to regional geochemical data: problems and possibilities. App Geochem. 2002;7(3):185–206.
Risso C, Scasso RA, Aparicio A. Presence of large pumice blocks on Tierra del Fuego and South Shetland Islands shorelines from 1962 South Sandwich Islands eruption. Mar Geol. 2002;186:413–22.
Robock A, Ammann CM, Oman L, Shindell D, Levis S, Stenchikov G. Did the Toba volcanic eruption of ~ 74ka BP produce widespread glaciation? J Geophys Res: Atmospheres (1984–2012). 2009;114(D10). doi:10.1029/2008JD011652.
Rose WI, Riley CM, Dartevelle S. Sizes and shapes of 10-Ma distal fall pyroclasts in the Ogallala Group Nebraska. J Geol. 2003;111(1):115–24.
Ryan WBF, Carbotte SM, Coplan JO, O'Hara S, Melkonian A, Arko R, et al. Global Multi-Resolution Topography synthesis. Geochem Geophys Geosys. 2009; 10(3). doi:10.1029/2008GC002332.
Saffer DM, Underwood MB, McKiernan AW. Evaluation of factors controlling smectite transformation and fluid production in subduction zones: application to the Nankai Trough. Island Arc. 2008;17(2):208–30.
Saffer DM, Lockner DA, McKiernan A. Effects of smectite to illite transformation on the frictional strength and sliding stability of intact marine mudstones. Geophys Res Lett. 2012;39:L11304. doi:10.1029/2012GL051761.
Saito S, Underwood MB, Kubo Y. Expedition 322 Scientists. Proceedings IODP 322, Tokyo Integrated Ocean Drilling Program Management, International Inc Washington DC. 2010. doi:10.2204/iodpproc3221042010.
Schacht U, Wallmann K, Kutterolf S, Schmidt M. Volcanogenic sediment–seawater interactions and the geochemistry of pore waters. Chem Geol. 2008; 249(3–4):321.
Schindlbeck JC, Kutterolf S, Freundt A, Scudder RP, Pickering KT, Murray RW. Emplacement processes of submarine volcaniclastic deposits (IODP Site C0011 Nankai Trough). Mar Geol. 2013;343:115–24. doi:10.1016/j.margeo.2013.06.017.
Schindlbeck JC, Kutterolf S, Freundt A, Straub SM, Wang K-L, Jegen M, et al. The Miocene Galápagos ash layer record of IODP Legs 334&344: Ocean-island explosive volcanism during plume-ridge interaction. Geology. 2015. doi:10.1130/G366451.
Scudder RP, Murray RW, Plank T. Dispersed ash in deeply buried sediment from the northwest Pacific Ocean: an example from the Izu-Bonin arc (ODP Site 1149). Earth Planet Sci Lett. 2009;284(3–4):639–48.
Scudder RP, Murray RW, Schindlbeck JC, Kutterolf S, Hauff F, McKinley CC. Regional-scale input of dispersed and discrete volcanic ash to the Izu-Bonin and Mariana subduction zones. Geochem Geophys Geosys. 2014;15(11):4369–79.
Severmann S, Johnson CM, Beard BL, German CR, Edmonds HN, Chiba H, et al. The effect of plume processes on the Fe isotope composition of hydrothermally derived Fe in the deep ocean as inferred from the Rainbow vent site Mid-Atlantic Ridge 36 14′ N. Earth Planet Sci Lett. 2004;225(1):63–76.
Shaw DM, Watkins ND, Huang TC. Atmospherically transported volcanic glass in deep-sea sediments: theoretical considerations. J Geophysi Res. 1974;79(21):3087–94.
Sibuet JC, Letouzey J, Barbier F, Charvet J, Foucher JP, Hilde TW, et al. Back arc extension in the Okinawa Trough. J Geophys Res: Solid Earth (1978–2012). 1987;92(B13):14041–63.
Sigurdsson H. Volcanic episodes and rates of volcanism. In: Sigurdsson H, Houghten HB, McNutt SR, Ryme H, Stix J, editors. Encyclopedia of volcanoes. New York: Academic Press; 1999. p. 271–9.
Sigurdsson H, Sparks RSJ, Carey SN, Huang TC. Volcanogenic sedimentation in the Lesser Antilles Arc. J Geol. 1980;88:523.
Sigurdsson H, Leckie RM, Acton GD, et al. Proceedings of the Ocean Drilling Program: Initial reports Volume 165. College Station Texas: Ocean Drilling Program; 1997. p. 865.
Sigurdsson H, Kelley RM, Carey S, Bralower T, King J. History of circum-Caribbean explosive volcanism: $^{40}Ar/^{39}Ar$ dating of tephra layers. Proc ODP Sci Results. 2000;165:299–314.
Simkin T, Fiske RS. Krakatau 1883: the volcanic eruption and its effects. Washington DC: Smithsonian Institution Press; 1983. p. 464.
Stern RJ, Kohut EJ, Bloomer SH, Leybourne M, Fouch M, Vervoort J. Subduction Factory processes beneath the Guguan Cross-chain Mariana Arc: no role for sediments are serpentinites important? Contrib Mineral Petrol. 2006;151:202–21.
Straub SM. Multiple sources of Quaternary tephra layers in the Mariana Trough. J Volcanol Geotherm Res. 1997;76(3–4):251–76.
Straub SM. The evolution of the Izu Bonin–Mariana volcanic arcs (NW Pacific) in terms of major element chemistry. Geochem Geophys Geosyst. 2003;4. doi:10.1029/2002GC000357.

Straub SM. Timescales and causes of secular change in the Izu Bonin–Mariana volcanic arcs. Geochim Cosmochim Acta. 2008;72 (12). A905 Goldschmidt Conference Vancouver Canada.
Straub SM, Layne GD. The systematics of boron isotopes in Izu arc front volcanic rocks. Earth Planet Sci Lett. 2002;198(1–2):25–39.
Straub SM, Layne GD. The systematics of chlorine fluorine and water in Izu arc front volcanic rocks: Implications for volatile recycling in subduction zones. Geochim Cosmochim Acta. 2003b;67(21):4179–203.
Straub SM, Layne GD. Decoupling of fluids and fluid-mobile elements during shallow subduction: evidence from halogen-rich andesite melt inclusions from the Izu arc volcanic front. Geochem Geophys Geosyst. 2003a;4. doi:10.1029/2002GC000349.
Straub SM, Schmincke HU. Evaluating the tephra input into Pacific Ocean sediments: distribution in space and time. Geol Rundsch. 1998;87(3):461–76.
Straub SM, Layne GD, Schmidt A, Langmuir CH. Volcanic glasses at the Izu arc volcanic front: new perspectives on fluid and sediment melt recycling in subduction zones. Geochem Geophys Geosyst. 2004;5:Q01007. doi:10.1029/2002GC000408.
Straub SM, Goldstein SL, Class C, Schmidt A. Mid-ocean-ridge basalt of Indian type in the northwest Pacific Ocean basin. Nat Geosci. 2009;2(4):286–9.
Straub SM, Goldstein SL, Class C, Schmidt A, Gomez-Tuena A. Slab and mantle controls on the Sr-Nd-Pb-Hf isotope evolution of the post 42Ma Izu-Bonin-volcanic Arc. J Petrol. 2010;51(5):993–1026.
Straub, SM, Woodhead, JD, Arculus, RJ. Temporal Evolution of the Mariana Arc: Mantle Wedge and Subducted Slab Controls Revealed with a Tephra Perspective. J Petrol. 2015. doi:10.1093/petrology/egv005.
Taira A. Tectonic evolution of the Japanese island arc system. Annu Rev Earth Pl Sc. 2001;29(1):109–34.
Tamura Y, Gill J, Tollstrup D, Kawabata H, Shukuno H, Chang Q, et al. Silicic magmas in the Izu-Bonin oceanic arc and implications for crustal evolution. J Petrol. 2009;50(4):685–723.
Tani K, Fiske RS, Tamura Y, Kido Y, Naka J, Shukuno H, et al. Sumisu volcano Izu-Bonin arc Japan: site of a silicic caldera-forming eruption from a small open-ocean island. Bull Volcanol. 2008;70:547–62.
Taylor SR, McLennan SM. The continental crust: its composition and evolution. Malden: Blackwell; 1985.
Tobin HJ, Kinoshita M. NanTroSEIZE: the IODP Nankai Trough seismogenic zone experiment. Sci Drill. 2006;2(2):23–7.
Underwood MB, Pickering KT. Clay-mineral provenance sediment dispersal patterns and mudrock diagenesis in the Nankai accretionary prism southwest Japan. Clays Clay Miner. 1996;44(3):339–56.
Völker D, Kutterolf S, Wehrmann H. Comparative mass balance of volcanic edifices at the Southern Volcanic Zone of the Andes between 33°S and 46°S. J Volcanol Geotherm Res. 2011;205:114–29. doi:10.1016/jjvolgeores201103011.
Völker D, Wehrmann H, Kutterolf S, Iyer K, Geersen J, Rabbel W, et al. Constraining input and output fluxes of the southern Central Chile Subduction Zone: water chlorine sulfur. Int J Earth Sci. 2014;103(7):2129–53. doi:10.1007/s00531-014-1002-0.
Volynets ON, Ponomareva VV, Braitseva OA, Melekestsev IV, Chen CH. Holocene eruptive history of Ksudach volcanic massif South Kamchatka: evolution of a large magmatic chamber. J Volc Geotherm Res. 1999;91(1):23–42.
Watson AJ. Volcanic Fe CO2 ocean productivity and climate. Nature. 1997;385: 587–8. doi:10.1038/385587b0.
White SM, Chamley H, Curtis DM, deVries Klein G, Mizuno A. Sediment synthesis: Deep Sea Drilling Project Leg 58 Philippine Sea. Init Rep DSDP. 1980;58:963–1014. doi:10.2973/dsdpproc581451980.
White JDL, Smellie JL, Clague DA. Introduction: A Deductive Outline and Topical Overview of Subaqueous Explosive Volcanism, in Explosive Subaqueous Volcanism (eds J.D.L. White, J.L. Smellie and D.A. Clague), American Geophysical Union, Washington, D.C; 2003. doi:10.1029/140GM01.
Woods AW, Wohletz KH. Dimensions and dynamics of co-ignimbrite eruption clouds. Nature. 1991;350:225–7.
Zhou L, Kyte FT. Sedimentation history of the South Pacific pelagic clay province over the last 85 million years inferred from the geochemistry of Deep Sea Drilling Project Hole 596. Paleoceanography. 1992;7(4):441–65.
Ziegler CL, Murray RW. Geochemical evolution of the central Pacific Ocean over the past 56 Myr. Paleoceanography. 2007;22(2). doi:10.1029/2006PA001321.
Ziegler CL, Murray RW, Hovan SA, Rea DK. Resolving eolian volcanogenic and authigenic components in pelagic sediment from the Pacific Ocean. Earth Planet Sci Lett. 2007;254(3):416–32.
Ziegler CL, Murray RW, Plank T, Hemming SR. Sources of Fe to the Equatorial Pacific Ocean from the Holocene to Miocene. Earth Planet Sci Lett. 2008;270:258–70.